JOURNAL OF GEOPHYSICAL RESEARCH, VOL. 102, NO. D21, PAGES 25,543-25,564, NOVEMBER 20, 1997

Evaluation of source gas lifetimes from stratospheric observations

C. M. Volk[1,2,3], J. W. Elkins[1], D. W. Fahey[4], G. S. Dutton[1,2], J. M. Gilligan[1,2,5], M. Loewenstein[6], J. R. Podolske[6], K. R. Chan[6], and M. R. Gunson[7]

Abstract. Simultaneous in situ measurements of the long-lived trace species N_2O, CH_4, CFC-12, CFC-113, CFC-11, CCl_4, CH_3CCl_3, H-1211, and SF_6 were made in the lower stratosphere and upper troposphere on board the NASA ER-2 high-altitude aircraft during the 1994 campaign Airborne Southern Hemisphere Ozone Experiment/ Measurements for Assessing the Effects of Stratospheric Aircraft. The observed extratropical tracer abundances exhibit compact mutual correlations that show little interhemispheric difference or seasonal variability except at higher altitudes in southern hemisphere spring. The environmental impact of the measured source gases depends, among other factors, on the rate at which they release ozone-depleting chemicals in the stratosphere, that is, on their stratospheric lifetimes. We calculate the mean age of the air from the SF_6 measurements and show how stratospheric lifetimes of the other species may be derived semiempirically from their observed gradients with respect to mean age at the extratropical tropopause. We also derive independent stratospheric lifetimes using the CFC-11 lifetime and the slopes of the tracer's correlations with CFC-11. In both cases, we correct for the influence of tropospheric growth on stratospheric tracer gradients using the observed mean age of the air, time series of observed tropospheric abundances, and model-derived estimates of the width of the stratospheric age spectrum. Lifetime results from the two methods are consistent with each other. Our best estimates for stratospheric lifetimes are 122 ± 24 years for N_2O, 93 ± 18 years for CH_4, 87 ± 17 years for CFC-12, 100 ± 32 years for CFC-113, 32 ± 6 years for CCl_4, 34 ± 7 years for CH_3CCl_3, and 24 ± 6 years for H-1211. Most of these estimates are significantly smaller than currently recommended lifetimes, which are based largely on photochemical model calculations. Because the derived stratospheric lifetimes are identical to atmospheric lifetimes for most of the species considered, the shorter lifetimes would imply a faster recovery of the ozone layer following the phaseout of industrial halocarbons than currently predicted.

1. Introduction

Source gases of natural and/or anthropogenic origin may influence the environment in two ways. First, they affect the chemical composition of the atmosphere, most importantly stratospheric ozone levels by providing sources of halogen, hydrogen, and nitrogen in the stratosphere. When these source gases are decomposed in the stratosphere, usually by photolysis and reactions with $O(^1D)$ or OH, the degradation products form reactive species that participate in the catalytic destruction of ozone [*Crutzen*, 1970; *Molina and Rowland*, 1974]. Second, most source gases are also very efficient "greenhouse gases"; that is, they contribute to global warming due to their radiative properties.

One of the prime factors determining the overall environmental impact of a compound of anthropogenic or natural origin is its atmospheric residence time or lifetime,

$$\tau_{atm} = \frac{\text{atmospheric burden}}{\text{atmospheric sink}} \quad (1)$$

The lifetime determines the global burden of a compound resulting from a given history of emissions and is therefore needed to assess the level of emission reductions necessary to stabilize and/or reduce current concentrations. Accordingly, the ozone depletion potential (ODP) [*Wuebbles*, 1983; *Solomon et al.*, 1992; *World Meteorological Organization (WMO)*, 1995] and the greenhouse warming potential (GWP) [*Fisher et al.*, 1990; Intergovernmental Panel on Climate Change (*IPCC*), 1995] are proportional to compound lifetime.

The stratospheric lifetime,

$$\tau_{strat} = \frac{\text{atmospheric burden}}{\text{stratospheric sink}}, \quad (2)$$

determines how rapidly reactive degradation products are released from the source gas in the stratosphere and is thus a measure of the compound's potential to harm stratospheric ozone. If tropospheric sinks are absent, as is the case for N_2O

[1] Climate Monitoring and Diagnostics Laboratory, National Oceanic and Atmospheric Administration (NOAA), Boulder, Colorado.
[2] Cooperative Institute for Research in Environmental Sciences, University of Colorado, Boulder.
[3] Now at the Institut für Meteorologie und Geophysik, J. W. Goethe-Universität Frankfurt, Germany.
[4] NOAA Aeronomy Laboratory, Boulder, Colorado.
[5] Now at the Department of Physics and Astronomy, Vanderbilt University, Nashville, Tennessee.
[6] NASA Ames Research Center, Moffett Field, California.
[7] Jet Propulsion Laboratory, California Institute of Technology, Pasadena.

Paper number 97JD02215.
0148-0227/97/97JD-02215$09.00

and the fully halogenated chlorofluorocarbons (CFCs), the stratospheric lifetime is identical to the atmospheric lifetime.

The lifetime of a source gas is determined by the spatial distribution of removal rates and the efficiency of transport between the sources at the surface and the dominant removal regions. For the most part, lifetimes are currently calculated by two-dimensional (2-D) chemistry-transport models using laboratory data for absorption cross sections and reaction rates. Typically, the models compute steady state distributions of mixing ratios and loss rates and compare calculated and observed abundances to validate the model [*e.g., Ko and Sze*, 1982; *Ko et al.*, 1991]. Alternatively, the lifetime can be calculated using observed global abundances and model-derived removal rates [*e.g., Johnston et al.*, 1979; *Minschwaner et al.*, 1993]. The uncertainties of the derived lifetimes arise from the uncertainty of modeled transport in the first approach, from the uncertainty in the observations in the second approach, and from the uncertainty in the calculated removal rates in both cases. Model-derived lifetimes currently differ by about 20% or more between different models [*Kaye et al.*, 1994].

Lifetimes of source gases can also be inferred from analysis of global emission inventories and observed tropospheric concentrations and trends [*Cunnold et al.*, 1994, 1997; *Elkins et al.*, 1993; *Fisher and Midgley*, 1994; *Prinn et al.*, 1995]. However, the accuracy and length of emission and concentration records is currently sufficient only for CFC-11 and CH_3CCl_3 to yield reliable lifetime estimates by these inverse methods [*Kaye et al.*, 1994]. The inverse methods and model results currently converge to a CFC-11 lifetime between 40 and 60 years. For CFC-12, however, inferred lifetimes range from 122 years [*Kaye et al.*, 1994] to 180 years [*Cunnold et al.*, 1994], while models calculate lifetimes between 100 and 123 years [*Kaye et al.*, 1994].

Apart from the above traditional approaches to calculate or infer lifetimes, a method to derive the ratio of the stratospheric lifetimes of two tracers has been proposed by *Plumb and Ko* [1992]. They showed that if the mixing ratios of two long-lived trace constituents, σ_1 and σ_2, are in steady state and universally correlated with each other everywhere in the lower stratosphere, then the slope of the correlation at the tropopause equals the ratio of the stratospheric removal rates of the compounds and thus

$$\frac{\tau_1}{\tau_2} \cong \frac{d\sigma_2}{d\sigma_1}\frac{B_1}{B_2} \tag{3}$$

where B_i is the total atmospheric burden for species i and τ_i is its stratospheric lifetime, equal to atmospheric lifetime for species without tropospheric sinks. In principle, this approach allows the determination of lifetime ratios directly from observations without the need to accurately describe atmospheric transport and chemistry or estimate emissions. Thus, it might serve to improve lifetime estimates for some species by relating them to a species with well-known lifetime, like CFC-11. Furthermore, since the ODP is defined relative to CFC-11, accurate estimates of lifetimes relative to the CFC-11 lifetime would be of direct use to refine ODPs. In practice, however, this method has not competed with the traditional approaches of determining lifetimes as few anthropogenic species are in steady state in the atmosphere and precise, simultaneous tracer observations necessary to determine a correlation slope in the lowermost stratosphere have been scarce.

In this paper we build on the theoretical work of *Plumb and Ko* [1992] and *Plumb* [1996] to reexamine the conditions for (3) to hold within a more complete conceptual model of stratospheric transport than was considered in the former two studies. We further propose a method of deriving the stratospheric lifetime of a long-lived tracer from its correlation with the "age" of stratospheric air. We present simultaneous in situ observations of N_2O, CH_4, CFC-12 (CCl_2F_2), CFC-113 ($CClF_2CCl_2F$), CFC-11 (CCl_3F), CCl_4, CH_3CCl_3, H-1211 ($CBrClF_2$), and SF_6 in the lower stratosphere and show that the data support the applicability of the concepts. We then build on formalisms of *Hall and Plumb* [1994] to develop a method to correct for the effects of transience, that is, tropospheric growth of tracer abundances, and finally apply the approach to derive stratospheric lifetimes for these long-lived species, and, with higher accuracy, their lifetimes relative to the lifetime of CFC-11.

2. Conceptual Framework

2.1. Flux-Gradient Relation

The fact that stratospheric lifetimes can be related to observable quantities in a simple manner in (3) owes to the fact that stratospheric transport is highly anisotropic; that is, it occurs preferably in certain directions. The global meridional circulation is the principle agent for vertical transport with air ascending in the tropics and descending at mid and high latitudes. Superimposed on this circulation, however, is faster quasi-horizontal transport by breaking planetary waves [*McIntyre and Palmer*, 1983], acting in the winter "surf zone" at midlatitudes on timescales of less than 3 months [*Boering et al.*, 1994]. Provided that this rapid quasi-horizontal mixing is much faster than vertical transport, *Mahlman et al.* [1986], *Holton* [1986], and *Plumb and Ko* [1992] pointed out two fundamental implications for species whose local lifetimes are long compared to horizontal mixing timescales (hereinafter simply referred to as "long-lived" species). First, their mixing ratios are homogenized along the same quasi-horizontal mixing surfaces such that their isopleths assume a common equilibrium shape, that is, are in "slope equilibrium." This explains why abundances of long-lived tracers in the lower stratosphere are tightly correlated with each other even as they fluctuate in time and space, a fact long borne out by observations [*Ehhalt et al.*, 1983; *Fahey et al.*, 1990; *Proffitt et al.*, 1989, 1990]. Second, the combined effect of vertical motion and horizontal mixing in the presence of horizontal gradients is equivalent to vertical diffusion, and transport can thus be described with a one-dimensional flux-gradient relation

$$F(Z) = -K(Z)\frac{d\chi}{dZ} \tag{4}$$

where $F(Z)$ is the global net tracer flux through an isopleth with altitude Z at a chosen reference latitude (*e.g.*, the equator), K is the effective mass-weighted vertical diffusion coefficient, and χ is the mixing ratio. Note that in the following we will generally use χ for mixing ratio, while σ will be used specifically for mixing ratios that are in steady state. (The advantage of this notation will become obvious later on.) For two steady species without stratospheric sources the flux through the tropopause equals the integrated sink above the tropopause, and (3) follows directly from (2) and (4) by the fact that K is not dependent on species.

The major violation to the idealized "global mixing" model described by *Plumb and Ko* [1992] is that horizontal transport is

not fast compared to vertical transport in the tropics. A number of tracer observations made from satellite [*Trepte and Hitchman*, 1992; *Randel et al.*, 1993], high-altitude aircraft [*Murphy et al.*, 1993; *Volk et al.*, 1996], and the space shuttle [*Michelsen et al.*, 1995] have suggested that the surf zone does not extend deep into the tropics. *Volk et al.* [1996] used differences between observed tropical and midlatitude correlations to deduce an average timescale for horizontal entrainment from the midlatitudes into the lower tropical stratosphere of 13.5 months, of the order or somewhat longer than the timescale for tropical ascent. Similar mixing times have been deduced from a combination of satellite and aircraft tracer data by *Minschwaner et al.* [1996] and *Hall and Waugh* [1997].

Plumb [1996] examined the opposite limit to global mixing, a "tropical pipe" model consisting of northern and southern hemispheric extratropical surf zones separated by an isolated tropical region, that is, excluding horizontal mixing into the tropics. In that model, an equation similar to (4) holds for the extratropical regions, with two important modifications [*Plumb*, 1996]: First, the flux through an isopleth is in general no longer completely diffusive but contains additional components representing the net detrainment flux from the tropics to the midlatitudes [*Plumb*, 1996, equation (13)]. However, this net detrainment vanishes at the tropopause, and the flux becomes purely diffusive there. Second, vertical tracer gradients and effective diffusion coefficients at the extratropical tropopause may differ between the hemispheres, and thus at the tropopause, (4) becomes

$$F(\chi_0) = -K_N \left.\frac{d\chi_N}{dZ}\right|_{\chi_0} - K_S \left.\frac{d\chi_S}{dZ}\right|_{\chi_0} \tag{5}$$

where χ_0 is the tropopause mixing ratio and the suffixes N and S denote the northern and southern extratropical surf zones, respectively. *Plumb* [1996] further showed that (5) may be split into two equations, separately relating the vertical gradient $d\chi/dZ$ in each extratropical region to the portion of the flux influencing each hemisphere. Similarly, for two long-lived tracers, (3) holds separately for the two hemispheres, relating the correlation slope in each hemisphere to the ratio of their (stratospheric) hemispheric lifetimes. Finally, if the correlation slopes in both hemispheres do not differ much from each other, (3) applied at the tropopause using an average correlation slope is likely to be a good approximation for the ratio of the global stratospheric lifetimes [*Plumb*, 1996].

In order to account for the fact that the tropics are in reality not completely isolated [*Avallone and Prather*, 1996; *Minschwaner et al.*, 1996; *Volk et al.*, 1996], one might extend the "tropical pipe" model to include horizontal entrainment from the midlatitudes into the tropics, as described by *Volk et al.* [1996]. The modifications to (4) in this "leaky pipe" model consist of yet another nondiffusive flux component representing the net entrainment into the tropics. However, this flux vanishes at the tropopause as long as mixing ratios of long-lived tracers are continuous across the tropopause, which can be considered a safe assumption. (The explicit mathematical justification for this statement proceeds in analogy to the derivation of *Plumb*'s [1996] equation (13), with an additional flux term that vanishes if mixing ratios approaching the tropopause from both sides equal each other.)

We note, however, that these nondiffusive fluxes above the tropopause generally cause inherent curvature in tracer-tracer correlations. In the idealized "global mixing" model described by *Plumb and Ko* [1992], two tracers are linearly correlated in any region of the stratosphere if their global fluxes are either constant or proportionally related with each other within that region; this applies, for example, to species in steady state with negligible local sources or sinks. In the "tropical pipe" and the more realistic "leaky pipe" models, however, linear correlations require in addition that the nondiffusive entrainment and detrainment fluxes across the tropical/midlatitude boundary in each hemisphere be either constant within the region of interest or change proportionally to the global fluxes for both species, neither of which there is reason to assume. Curvature in correlations may thus be expected even in the absence of local chemical sinks or growth.

In summary, the conclusions of *Plumb* [1996] are not undermined in the more realistic case of substantial, but incomplete, isolation of the tropical region. Equation (5) holds at the tropopause (but only there) if the tracer is in slope equilibrium at and just above the extratropical tropopause in each hemisphere. Equation (3) holds at the tropopause if, in addition, the interhemispheric difference between the extratropical correlation slopes is small. Note that the global tracer fluxes through the tropopause are related to extratropical vertical gradients; no information about tropical mixing ratios is needed. Finally, note that, for reasons discussed by *Plumb* [1996], the vertical gradients should be derived from data taken during the winter half year that dominates net transport.

2.2. Global Fluxes and the Mean Age of the Air

The transit time of an air parcel since its entry to the stratosphere has been termed the "age" of stratospheric air [*Bischof et al.*, 1985; *Schmidt and Khedim*, 1991]. *Hall and Plumb* [1994] pointed out that, due to the diffusive nature of stratospheric transport, air parcels are not characterized by a unique age, but are composed of many components with different ages. Each air parcel then may be associated with a spectrum of the ages of its irreducible elements. In fact, *Hall and Plumb* [1994] identified this age spectrum with the Green's function of the continuity equation for a conserved tracer, such that the mixing ratio $\chi(\mathbf{x},t)$ of a conserved tracer at location $\mathbf{x}$ = (latitude, longitude, altitude) and time t in the stratosphere is given by

$$\chi(\mathbf{x},t) = \int_0^\infty \chi_0(t-t')G(\mathbf{x},t')dt' \tag{6}$$

where $G(\mathbf{x},t')$ is the age spectrum at location $\mathbf{x}$ and $\chi_0(t)$ is the mixing ratio at the point of entry to the stratosphere, usually identified with the tropical tropopause. While the age spectrum is not directly accessible from observable quantities, its first moment, the mean age (or simply "age"),

$$\Gamma(\mathbf{x}) = \int_0^\infty t' G(\mathbf{x},t')dt' , \tag{7}$$

is readily identified with the lag time between stratospheric and tropospheric mixing ratios of a linearly growing, conserved tracer [*Hall and Plumb*, 1994]. We will hereinafter refer to such tracers as "chronological tracers."

In the following, we will make variable use of the concepts of age spectrum and mean age. One central assumption will be that there exists a unique functional relationship at and just above the extratropical tropopause between the mean age of an air parcel

and its mixing ratio of a long-lived tracer. Since mean age is a unique function of the mixing ratio of a chronological tracer, this is equivalent to requiring universal correlations between chronological and long-lived tracers. If the dynamical prerequisites for slope equilibrium are given, such as the predominance of quasi-horizontal mixing over vertical transport, then chronological tracers as well as tracers with spatially uniform sinks are theoretically in exact slope equilibrium. (This can be verified from the slope budget analysis of *Plumb* [1996, Appendix]). Spatially varying sinks, however, generally cause deviations from slope equilibrium (and thus noncompact correlations), unless they act on timescales much slower than horizontal mixing timescales. Moreover, even if both tracers are in slope equilibrium, interhemispheric differences in stratospheric transport can result in interhemispheric differences in tracer-tracer correlations [*Plumb*, 1996]. In how far correlations between chronological and long-lived tracers are universal in practice will be discussed in more detail in the next section by examining the observations.

For the moment, we require a slightly less stringent condition, namely that there exist functional relations $\chi(\Gamma)$ between tracer mixing ratio and mean age just above the extratropical tropopause in each hemisphere separately, but with equal gradients $d\chi/d\Gamma$ at the tropopause. We can then rewrite (5) as

$$F(\chi_0) = -\left.\frac{d\chi}{d\Gamma}\right|_{\chi_0} \cdot \left(K_N \left.\frac{d\Gamma_N}{dZ}\right|_{\chi_0} + K_S \left.\frac{d\Gamma_S}{dZ}\right|_{\chi_0} \right). \quad (8)$$

Small differences in the hemispheric tropopause gradients $d\chi/d\Gamma$ can be accommodated with little error by using the average value. For example, for a 20% interhemispheric difference in the gradients, use of the average gradient $d\chi/d\Gamma$ in (8) would introduce a maximum error of 10% in the global flux $F(\chi_0)$ only if stratospheric transport were completely dominated by one hemisphere (*e.g.*, if $K_S = 0$); it would yield the correct flux if transport were symmetric (that is, $K_S = K_N$). In reality, transport is stronger in the northern hemisphere by about a factor of 2 [*Rosenlof and Holton*, 1993], such that an error of a few percent is introduced (for a 20% difference of hemispheric gradients) by substituting either the average of the hemispheric gradients or the northern hemisphere gradient for $d\chi/d\Gamma$ in (8).

In order to make practical use of (8), the term in parentheses on the right hand needs to be evaluated. This term can be eliminated by considering (8) for a chronological tracer, that is, a conserved tracer whose tropospheric time history is given by

$$\chi_0(t) = \begin{cases} 0 & t<0 \\ bt & \text{otherwise} \end{cases}. \quad (9)$$

For large t then, the mixing ratio anywhere in the stratosphere is

$$\chi(\mathbf{x},t) = b\cdot\left(t - \Gamma(\mathbf{x})\right) \quad (10)$$

where stratospheric transport is assumed to be stationary in the annual mean, such that the mean age at a given location is independent of time. The net flux through the tropopause of a conserved tracer must be balanced by its accumulation rate above the tropopause, thus the left-hand side of (8) now becomes

$$F(\chi_0) = \int_u \rho \frac{\partial \chi}{\partial t} d^3\mathbf{x} = b \int_u \rho d^3\mathbf{x} = b M_u \quad (11)$$

where ρ is air density, M is air mass, and u refers to the upper atmosphere, here the region above the χ_0-isopleth, which is by definition identical to the tropopause. On the right-hand side of (8), we substitute $d\chi/d\Gamma = -b$ and thus obtain

$$M_u = \left(K_N \left.\frac{d\Gamma_N}{dZ}\right|_{\chi_0} + K_S \left.\frac{d\Gamma_S}{dZ}\right|_{\chi_0} \right). \quad (12)$$

This equation, although derived by considering a chronological tracer, is in fact tracer-independent. We can thus substitute it into (8) and obtain for any long-lived tracer

$$F(\chi_0) = -\left.\frac{d\chi}{d\Gamma}\right|_{\chi_0} M_u . \quad (13)$$

Knowledge of the tracer gradient with respect to mean age at the extratropical tropopause thus allows one to directly calculate the net global tracer flux through the tropopause. For long-lived tracers in steady state (with mixing ratios σ) and without stratospheric sources, the stratospheric lifetime can then be derived via

$$\frac{B}{\tau} = -\left.\frac{d\sigma}{d\Gamma}\right|_{\sigma_0} M_u . \quad (14)$$

3. Airborne In Situ Observations

3.1. ASHOE/MAESA Campaign

The measurements presented here were obtained simultaneously on board the NASA ER-2 aircraft during the aircraft campaign Airborne Southern Hemisphere Ozone Experiment/Measurements for Assessing the Effects of Stratospheric Aircraft (ASHOE/MAESA). The mission consisted of transit flights between Moffett Field, California (37°N, 122°W), and Christchurch, New Zealand (44°S, 172°E), in March 1994 and return in late October/early November 1994, two local flights during each transit from Hawaii (20°N, 155°W), and several poleward and equatorward flights from Christchurch during each of the four field deployments of ASHOE. Each deployment lasted approximately 3 weeks, in March/April, May/June, July/August, and October 1994. A northbound flight from Moffett Field concluded the campaign on November 4, 1994. An overview of the campaign is given by *Tuck et al.* [1997b].

A new instrument on board the ER-2, the Airborne Chromatograph for Atmospheric Trace Species (ACATS-IV) measured CFC-11, CFC-12, CFC-113, CCl_4, CH_3CCl_3, H-1211, and CH_4 once every 3 min, and N_2O and SF_6 once every 6 min. ACATS-IV is a four-channel gas chromatograph with electron capture detection (GC/ECD). The instrument is described by *Elkins et al.* [1996a]. Data reduction methods, corrections for detector nonlinearity and internal contaminations, and the instrumental precision determined for each flight and compound are discussed in detail by *Volk* [1996]. The precision uncertainties improved during the course of the mission and were generally less than 3% (1 s.d.) [cf. *Elkins et al.*, 1996a, Table 2]. The accuracy of the calibration is set by the accuracy of the standard mixtures used in-flight. These bulk standards are referenced to gravimetric standards prepared at our laboratory in Boulder, with an accuracy of less than 2%. Note, however, that the uncertainty in the absolute calibration scale does not affect

the lifetime determination with the use of (3) and (4) as long as all tracer data used to derive the vertical gradient and the global burden are referenced to the same calibration scale.

During ASHOE/MAESA, ACATS-IV provided data on 22 flights, each typically lasting 8 hours. The instrument was configured to measure SF_6 and H-1211 only during the last deployment; quality data for these species are thus only available for the last 7 and 8 flights, respectively, between October 13 and November 4, 1994. The ASHOE/MAESA observations constitute the most extensive data set ever reported for the species measured by ACATS-IV, spanning latitudes from 60°N to 70°S during northern hemisphere spring and fall, and southern hemisphere fall, winter, and spring. The observations also comprise the first real-time in situ measurements of CCl_4, CH_3CCl_3, H-1211, H_2, and SF_6 in the stratosphere.

High-frequency N_2O measurements (once every second) were obtained by the Airborne Tunable Laser Absorption Spectrometer (ATLAS) on board the ER-2 [*Podolske and Loewenstein*, 1993]. The nominal instrumental accuracy is 5% (1 s.d.), while flight-to-flight repeatability of upper tropospheric measurements during ASHOE/MAESA indicates an instrumental precision of about 1% (1 s.d.). ATLAS and ACATS-IV N_2O measurements agreed well within their respective uncertainties. Because ACATS-IV sampled N_2O only every 6 min, we will use ATLAS data in the analysis presented here. The data were averaged into 10-s intervals synchronous with the ACATS-IV sampling times.

3.2. Observed Tracer Correlations

As expected, mixing ratios of long-lived tracers measured during ASHOE/MAESA are generally well correlated throughout the lower stratosphere. In the following discussion, we will distinguish between the terms "compactness" and "universality" of correlations. "Compactness" shall be used here as a qualifier for any given correlation diagram and simply signify that the scatter of a correlation curve is small. "Universality," on the other hand, shall indicate compactness on a wide temporal and spatial scale, meaning little scatter in a correlation diagram containing data from all seasons and from a large spatial region (here generally the extratropical lower stratosphere, unless otherwise specified).

Although tracer correlations obtained in individual regions of the lower stratosphere are mostly compact, they are not necessarily universal over all latitudes. Tropical correlations between some tracers are observed to differ from midlatitude correlations because rapid horizontal mixing does not penetrate into the tropics [*Volk et al.*, 1996]. These deviations have already been discussed. More generally, slope equilibrium and thus the universality of tracer correlations break down where horizontal mixing is not fast compared to either local sources and sinks or vertical transport [*Plumb and Ko*, 1992]. In the former case the tracer distribution is influenced by local chemistry, while in the latter the effects of remote chemistry are communicated by vertical transport too fast to be horizontally homogenized. For the species considered here, with the exception of H-1211, the bulk of the removal occurs in the middle and upper stratosphere; local chemistry in the lower midlatitude stratosphere is very slow and should thus not be of concern.

Hall and Prather [1995] examined the correlation between N_2O and a chronological tracer in a three-dimensional transport model and found departures from universality, even in the lower midlatitude stratosphere. This could be an indication that the dynamical prerequisites for slope equilibrium are not met even in the lower stratosphere. However, the model used in that study has rather low resolution such that the nonuniversal correlations could also be due to a blurring of the tropical/extratropical differences in tracer structure over a wider latitude band.

The spatial and temporal range of the ASHOE/MAESA data allow us to examine the universality (or lack thereof) of tracer correlations in the real stratosphere, and thus to test whether the assumptions made in the derivation of (3) and (14) apply. In particular, we seek to establish that (i) the long-lived tracers considered exhibit universal correlations with each other in each hemisphere, (ii) that the same holds for correlations of a chronological tracer with these long-lived tracers such that their mixing ratios are uniquely correlated with mean age, and (iii) that interhemispheric differences in all correlation slopes are small. We reemphasize that these prerequisites need be met only in a thin (but finite) layer above the extratropical tropopause. The eventual breakdown of the correlations' universality at some higher altitude or in the tropics would not undermine the validity of (3) and (14).

We consider only extratropical data throughout this paper. Tropical air was identified for each flight as the region equatorward of the sharp meridional gradients in the NO_y/O_3 ratio observed in the subtropics [*Murphy et al.*, 1993; *Fahey et al.*, 1996]. Figure 1 shows the phase space covered by the observations used in this work; that is, it shows locations in latitude-height space (using potential temperature, Θ, as vertical coordinate) and approximate times of all extratropical (stratospheric and upper tropospheric) CFC-11 observations collected by ACATS-IV during the mission.

3.2.1. Correlations between long-lived tracers. Departures from universality are most pronounced for correlations of two tracers with distinctly different spatial distributions of sources and sinks [*Plumb*, 1996; *Volk et al.*, 1996]. The long-lived tracers considered here fall into two groups: very long-lived species (N_2O, CH_4, CFC-12, and CFC-113) with a maximum loss region located at an altitude of about 30 km, and the shorter-lived

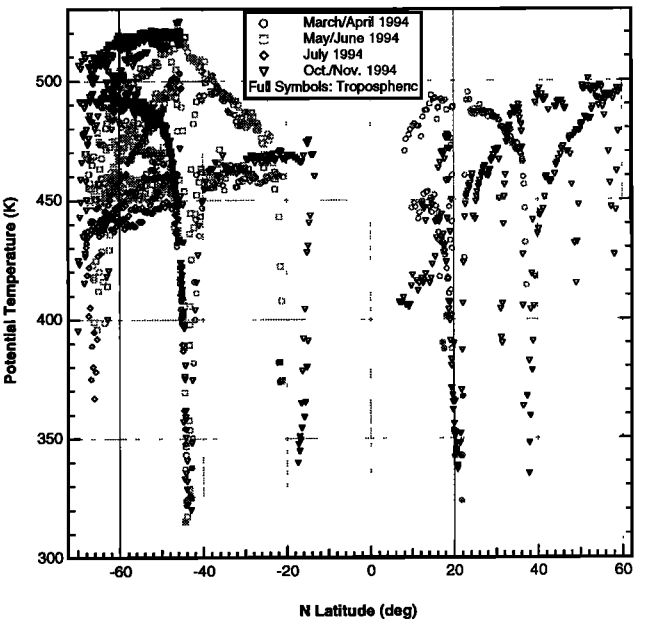

Figure 1. Locations in potential temperature-latitude space and approximate times of all extratropical tropospheric (solid symbols) and stratospheric (open symbols) observations of CFC-11 taken by ACATS-IV during ASHOE/MAESA.

species (CFC-11, CCl_4, CH_3CCl_3, and H-1211) that experience their maximum loss below 25 km [e.g., *Minschwaner et al.*, 1993]. The shorter lifetimes of the latter group are, of course, a direct consequence of the loss at lower altitudes. Obviously, departures from universality will be most easily detectable in correlations between a very long-lived and a shorter-lived tracer, and will not depend much on the specific choice of tracer from each group.

The tracer pair most suitable for inspection is CFC-11 and N_2O, both of which were measured with high precision throughout the mission. We examine the extratropical CFC-11–N_2O correlation for each hemisphere and each deployment of ASHOE/MAESA in Figure 2. There is no detectable interhemispheric difference in March/April nor a detectable transience of the southern hemispheric correlation from April through July. All the data from the first three deployments (Figures 2b-2e) follow the same reference curve, obtained from a quadratic fit to all ASHOE/MAESA observations except the southern hemisphere spring observations (Figure 2a). A small deviation from this reference curve is apparent in the northern hemisphere fall at low N_2O levels (Figure 2f). A much larger deviation in the opposite direction occurs in the southern hemisphere spring correlation (Figure 2g) for observations taken above Θ475 K. The lower altitude data (Θ<475 K) still follow the reference correlation. Dividing the data along the Θ = 475 K isentrope was found to best separate the two correlation branches in Figure 2g. In contrast, dividing the data into latitude bins or into vertical and horizontal flight legs did not achieve this separation, nor did it reveal any systematic structure in the correlations of Figures 2b-2f.

Note that the departure from universality of the southern hemisphere spring correlation between CFC-11 and N_2O is opposite in direction to the one observed in northern midlatitudes on May 7, 1993, during the Stratospheric Photochemistry,

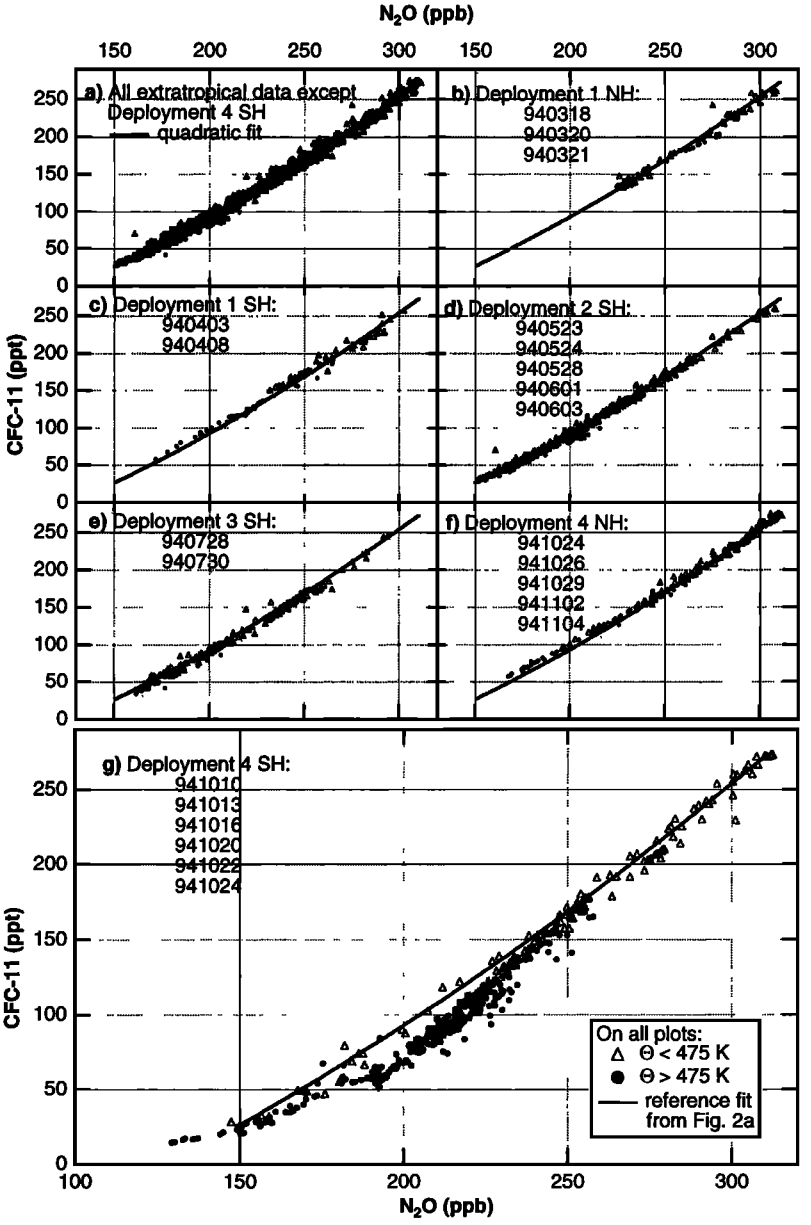

Figure 2. Correlation between CFC-11 and N_2O mixing ratios, separated by hemisphere (NH and SH), by deployment of ASHOE/MAESA and by potential temperature (Θ) as indicated.

Aerosols, and Dynamics Expedition (SPADE) campaign [*Waugh et al.*, 1997a]. We believe that the present pattern arises for different reasons, namely as a consequence of strong winter descent of air from high altitudes where the correlation is nonuniversal due to significant removal of CFC-11 or of both species. Quasi-horizontal mixing is apparently not fast enough compared to the descent to reestablish universality above Θ = 475 K. The lack of a similar feature in the observations taken in late July (Figure 2e) may indicate that polar descent has only become strong in late winter (as is usually the case for the southern hemisphere), or it may simply owe to the fact that lower Θ levels (mostly below 475 K; see Figure 1) were spanned during the two July dates sampled by ACATS-IV.

The observations do not show evidence for either interhemispheric differences or significant transience throughout fall, winter, and spring, of the CFC-11–N_2O correlation below Θ = 475 K. The fact that the ER-2 obtained both vertical and horizontal profiles at a wide range of latitudes (Figure 1) suggests that the CFC-11 versus N_2O correlation is indeed universal throughout this lowest part of the extratropical stratosphere, and that the prerequisites for the applicability of (3) are satisfied for this pair of tracers. Other correlations between very long-lived and shorter-lived species behave similarly to the CFC-11–N_2O correlation, while correlations between two very long-lived or two shorter-lived species show no detectable seasonal or interhemispheric variations even above Θ = 475 K as their sink structures are more similar to each other than those of CFC-11 and N_2O.

H-1211 assumes a special position among the shorter-lived species in that it is photolyzed not only in the ultraviolet, but also in the visible range [*Kaye et al.*, 1994]. As a consequence, a considerable amount of H-1211 is removed in the troposphere, and local lifetimes in the lower stratosphere are short. For comparison, the radiative transfer model of *Minschwaner et al.* [1993] calculates annually averaged local lifetimes shorter than 1 year for H-1211 and shorter than 3.5 years for CFC-11 equatorward and upward of 30°N and 20 km altitude (R. J. Salawitch, personal communication, 1995). Departures from universality in correlations between H-1211 and longer-lived compounds might thus be expected already at lower altitudes.

Figure 3 shows the correlation between H-1211 and N_2O for both hemispheres during October/November 1994. There is no evidence for interhemispheric differences at the lower Θ levels. As in the case of CFC-11 versus N_2O, however, a departure from universality is observed in the southern hemisphere at higher altitudes. The deviating correlation could be separated best by dividing the southern hemispheric data along the 460 K isentrope instead the 475 K isentrope. The fact that departure from universality is observed already at this lower Θ level is consistent with the influence of local chemistry at lower altitudes for H-1211 than for CFC-11. Another indication of significant local chemistry is that the correlation exhibits noticeable curvature already at low altitudes. The correlation is nonetheless remarkably compact just above the tropopause, and interhemispheric differences there are small. Seasonal variations cannot be examined since H-1211 was not measured until the last deployment. However, because of the similar behavior of H-1211 and CFC-11 during the fourth deployment, it is fair to assume that seasonal variations of H-1211 with respect to N_2O at low altitudes will be similarly small as for CFC-11.

3.2.2. Correlations of long-lived tracers with SF_6. Among the tracers measured by ACATS-IV, SF_6 forms its own category. It

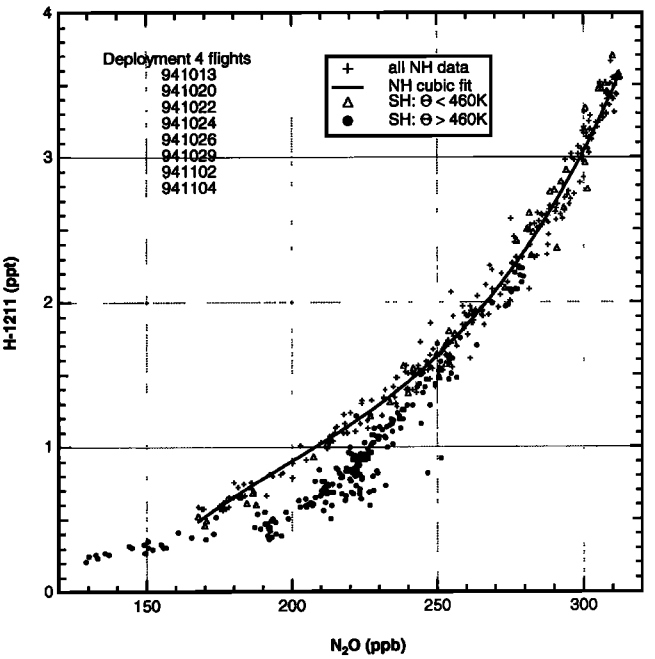

Figure 3. Correlation between H-1211 and N_2O mixing ratios during the fourth deployment of ASHOE/MAESA, binned by hemisphere and by potential temperature as indicated.

is an essentially conserved tracer whose decline with altitude in the stratosphere is due not to photochemical loss, but to tropospheric growth. As will be discussed in section 4.1, SF_6 is very close to being a truly chronological tracer. Linear growth has the same effect on tracer distributions as a spatially uniform sink; the effective sink structure of SF_6 thus differs drastically from that of the long-lived tracers whose sinks are essentially confined to the tropics. One might therefore expect larger departures from universality in correlations of long-lived tracers with SF_6 than in correlations between long-lived tracers.

Figure 4 shows the correlations between SF_6 and N_2O, CFC-11, and H-1211 during October/November 1994 separated by hemisphere; the southern hemisphere data are again divided along the 475 K isentrope. Two features in these correlations deserve notice. First, the southern hemisphere mixing ratios of all three tracers in Figure 4 above 475 K are lower than the mixing ratios below 475 K for a given SF_6 mixing ratio. This departure from universality is the same as already identified in the correlations between the long-lived tracers. Another feature, not present for the correlations between long-lived tracers, is an interhemispheric asymmetry, most pronounced for the N_2O-SF_6 correlation, less so for CFC-11 versus SF_6, and least pronounced for H-1211 versus SF_6. The observed asymmetry is greatest in the lower altitude range (Θ<475 K), where SF_6 values in the northern hemisphere are up to 5-10% higher than in the southern hemisphere on a given N_2O surface.

One explanation for this interhemispheric difference might be that it is driven by the tropospheric interhemispheric asymmetry for SF_6 of approximately 10% [*Geller et al.*, 1997]. *Tuck et al.* [1997a] indeed suggest, based on interhemispheric differences of CO, NO_y, and condensation nuclei, that the stratosphere in each hemisphere receives a dominant fraction of its air from its own troposphere. In this case one might expect the hemispheric correlations to diverge as they approach the tropopause. The correlations displayed in Figure 4 seem to suggest the opposite,

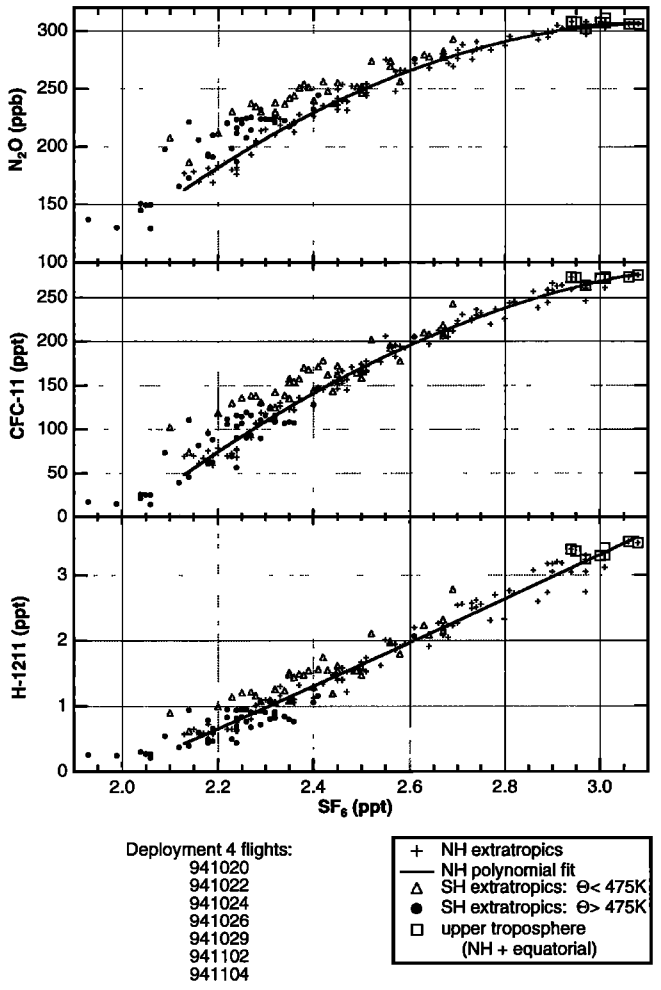

Figure 4. Correlations between mixing ratios of long-lived tracers (N_2O, CFC-11, and H-1211) and SF_6 during the fourth deployment of ASHOE/MAESA, binned by hemisphere and by potential temperature as indicated.

but the evidence is inconclusive. No SF_6 observations below 15.5 km are available in the southern hemisphere due to instability of the ACATS-IV SF_6 channel on its first few flights during the ascents and descents. Only eight SF_6 samples were taken in the upper troposphere, four at northern midlatitudes and four within 4° of the equator, with each group yielding an average of ~3.0 ppt (Figure 4). However, H-1211 measurements were taken upward from the upper troposphere in both hemispheres. The apparent lack of an interhemispheric asymmetry in the low altitude branch of the H-1211 versus N_2O correlation (Figure 3), despite the ~10% asymmetry in tropospheric H-1211, argues against significant influence of the tropospheric asymmetry on the stratosphere. Perhaps even stronger evidence against such influence comes from the observation that the annual cycles of CO_2 in the two hemispheres are in phase in the lower stratosphere [*Boering et al.*, 1996], although out of phase in the troposphere.

More likely, the interhemispheric differences in the correlations simply arise from asymmetries of stratospheric transport. The "tropical pipe" model of *Plumb* [1996], for example, predicts different correlation slopes at the tropopause in each hemisphere if asymmetries in transport are introduced and sinks are prescribed globally. (This case also applies to SF_6 whose linear growth acts analogous to a globally uniform sink.) Interestingly, that difference disappears if sinks in the model are confined to the tropics; this again is consistent with our observations showing no detectable interhemispheric difference at the tropopause for correlations between long-lived tracers with essentially tropical sinks (compare previous section). The observed interhemispheric differences in the correlations with SF_6 are also qualitatively consistent with three-dimensional simulations with the model used by *Waugh et al.* [1997b]. On a given age surface, that model produces lower N_2O in the southern than in the northern hemisphere throughout all seasons (T. Hall and D. Waugh, personal communication, 1997).

Our main concern here are the interhemispheric differences of the correlation slopes at the tropopause that were assumed to be small in the derivation of (14). The largest differences would occur if the hemispheric correlations immediately diverge upward from the tropopause, in which case the hemispheric correlation slopes at the tropopause would differ by about 20% for N_2O versus SF_6 and less for the shorter-lived compounds versus SF_6. Even if it were present in the annual mean, a difference of this magnitude would not introduce a sizable error into the lifetime calculation, as discussed in section 2.2.

4. Methods

Although the derivation of stratospheric lifetimes from the observations by use of the concepts outlined in section 2 appears to be a fairly straightforward matter, there are some major difficulties to overcome in practice if the results are to be anything more than a rough estimate. Particular attention is required by the fact that the species considered are not in steady state, but generally nonlinearly growing in the atmosphere. This section will describe in detail the steps necessary in order to apply (3) and (14) to the observations at hand.

4.1. Mean Age of the Air Calculation

The ideal tracer for the determination of the mean age of a stratospheric air parcel is completely conserved in the stratosphere and exhibits tropospheric growth that is large, linear, and accurately known. Tracers used to derive the age are CO_2 [*Bischof et al.*, 1985; *Schmidt and Khedim*, 1991; *Woodbridge et al.*, 1995; *Boering et al.*, 1996], CFC-115 [*Pollock et al.*, 1992; *Daniel et al.*, 1996], and recently SF_6 [*Elkins et al.*, 1996a; *Harnisch et al.*, 1996]. The use of CO_2 as an age tracer in the lowermost stratosphere is complicated by its tropospheric annual cycle [*Hall and Prather*, 1993], while large uncertainties in the tropospheric time series of CFC-115 limit the age determination from CFC-115 to an accuracy of about 1 year [*Daniel et al.*, 1996].

SF_6 most closely matches all the requirements for an accurate age determination. Its lifetime is about 3200 years [*Ravishankara et al.*, 1993], its tropospheric time series is very well established by in situ measurements from a number of locations around the globe, and its growth rate of approximately 8% $year^{-1}$ (in 1994) yields good age resolution for stratospheric SF_6 measured with a precision of few percent. SF_6 is nearly a chronological tracer in the sense defined above, its growth over the past 10 years being only slightly nonlinear. A global mean time series has recently been compiled [*Geller et al.*, 1997] using combined intercalibrated measurements from *Maiss et al.* [1996] and from the National Oceanic and Atmospheric

Administration/Climate Monitoring and Diagnostics Laboratory (NOAA/CMDL) network of global surface stations:

$$\overline{[SF_6]}(t) = 3.4361 + 0.2376(t-1996) + 0.0049(t-1996)^2 \quad (15)$$

where t is the year (between 1987 and 1996) and the mixing ratio is given in ppt.

For a strictly chronological tracer, the mean age Γ corresponds to the lag time between stratospheric and tropopause mixing ratios [*Hall and Plumb*, 1994]:

$$\chi(\mathbf{x},t) = \chi_0\left(t - \Gamma(\mathbf{x})\right) \quad (16)$$

Although the nonlinearity of the SF_6 time series is small, it causes the true age Γ to systematically differ from this lag time. We describe here a more general method for calculating the mean age from a conserved, quadratically growing tracer, and then examine the magnitude of the difference between the mean age and the lag time. Consider a tropospheric time series of the form

$$\chi_0(t) = a + b\cdot(t-t_0) + c\cdot(t-t_0)^2 \ . \quad (17)$$

Substituting χ_0 into (6) and using (7) yields

$$\chi(\mathbf{x},t) = \chi_0\left(t - \Gamma(x)\right) + 2c\Delta^2(\mathbf{x}) \quad (18)$$

where Δ is the width (second moment) of the age spectrum, as defined by *Hall and Plumb* [1994]:

$$\Delta^2(\mathbf{x}) = \frac{1}{2}\int_0^\infty (t-\Gamma)^2 G(\mathbf{x},t)\,dt \ . \quad (19)$$

In passing, we note that (18) might in principle serve to infer the spectral width Δ from a sufficiently nonlinearly growing conserved tracer if the mean age Γ is already known, for example, by means of (16) from observations of a true chronological tracer. Here, however, our goal is to approximate Δ in order to derive the age from (18), which takes into account the nonlinearity of the tropospheric time series of SF_6. In the one-dimensional global diffusion limit, χ is uniquely related with Γ, and therefore Δ in (18) must be a function of Γ. In fact, for the simple case of one-dimensional mass-weighted diffusion with constant diffusion coefficient K and scale height H, it is $\Delta^2 = \Gamma H^2/K$, as shown by *Hall and Plumb* [1994]. One might therefore expect a simple relationship to hold between Δ and Γ in the lower stratosphere. Indeed, the timescale Δ^2/Γ in the Goddard Institute for Space Studies (GISS) general circulation model (GCM) runs performed by *Hall and Plumb* [1994] varies little throughout the stratosphere. The same holds for another GCM, the middle atmosphere version of the National Center for Atmospheric Research (NCAR) community climate model (MACCM2) (T. M. Hall and D. W. Waugh, personal communication, 1996). The latter model, which has higher resolution than the GISS GCM and yields ages in good agreement with the ones derived from our SF_6 observations [*Waugh et al.*, 1997b], shows $\Delta^2/\Gamma \approx 1.5$ years throughout the lower stratosphere, where Γ is defined as age with respect to tropical surface sources. The lower resolution GISS model obtains only about half this value, but also shows vertical age gradients that are too weak [*Hall and Plumb*, 1994]. We will make use of this relationship hereafter to parameterize Δ in terms of Γ, defining

$$\frac{\Delta^2}{\Gamma + \delta\Gamma} \equiv \Lambda \quad (20)$$

where we adopt a value of $\Lambda = 1.25 \pm 0.5$ years (a subjectively weighted average of the values obtained in the two GCMs) and $\delta\Gamma$ is the time lag between the (tropical) surface and the tropopause (since we define the age with respect to the tropopause). We can infer $\delta\Gamma$ from the time series of SF_6 global mean surface concentrations (essentially identical to average tropical surface values) and the average upper tropospheric SF_6 mixing ratio of 3.0 ppt (Figure 4) measured by ACATS-IV between October 20 and November 4, 1994. The global mean time series reached 3 ppt in January 1994, thus the time lag of the average tropopause mixing ratios with respect to the global mean surface time series is $\delta\Gamma = 0.8$ years. Although such a time lag may seem long compared to tropospheric mixing times, it is comparable with the time lag between tropical surface and tropopause mixing ratios obtained in the three-dimensional model simulation of *Hall and Plumb* [1994]. A similarly long time lag between the global surface mean and the tropopause is inferred from recent high-resolution vertical profiles of SF_6 obtained by a balloon-borne in situ gas chromatograph developed in our laboratory (F. L. Moore, personal communication, 1996).

Using (15), (18), and (20), the mean age Γ with respect to the tropopause of an air parcel observed at time t and location $\mathbf{x}$ is now derived by inverting the following relationship between the stratospheric mixing ratio of SF_6 and Γ:

$$[SF_6](\mathbf{x},t) = \overline{[SF_6]}\left(t - \Gamma - \delta\Gamma\right) + 2\Lambda c\cdot\left(\Gamma + \delta\Gamma\right) \quad (21)$$

where the mixing ratios are given in ppt, $\delta\Gamma = 0.8$ years, $\Lambda = 1.25 \pm 0.5$ years, and $c = 0.0049$ ppt year^{-2}. Figure 5 shows the mean ages calculated from (21) versus SF_6 mixing ratios of all observations during ASHOE/MAESA. The error bars reflect the precision of the SF_6 observations evaluated on a by-flight basis,

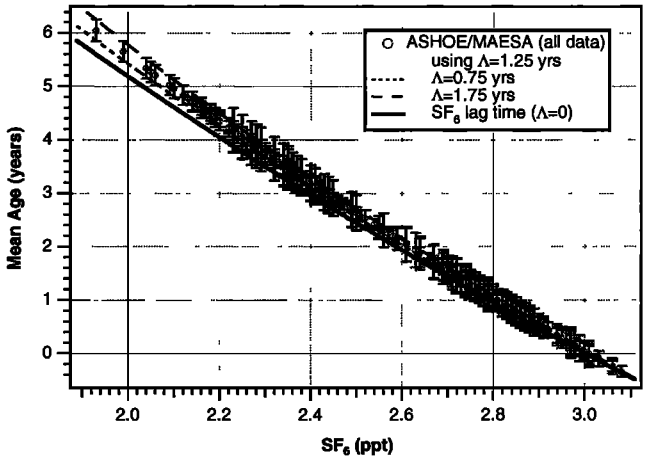

Figure 5. Age of the air and its uncertainty as derived from equation (21) for all SF_6 observations from seven flights of ASHOE/MAESA in October/November 1994. Error bars indicate the random uncertainty due to the precision of the SF_6 measurements. Dashed and dotted lines indicate the systematic uncertainty due to the uncertainty in the width of the age spectrum. The lag time derived from equation (16) is shown for comparison.

improving with time to about 0.04 ppt (corresponding to an age uncertainty of 2-3 months) during the last few flights. The systematic uncertainty in the inferred age resulting from the uncertainty in Λ (0.5 years) is comparable to the precision of the age values. Also shown is the lag time, that is, the age derived from the simpler relation (16), ignoring the nonlinearity of the SF_6 time series. The difference between the mean age and the lag time becomes significant for air older than 3-4 years and approaches 0.5 years for the oldest air (Γ= 6 years) measured.

4.2. Determination of Correlation Slopes

Equations (3) and (14) require knowledge of the gradient with respect to age ($d\chi/d\Gamma$) and the slope of the correlation between two species ($d\chi_1/d\chi_2$), respectively, at the extratropical tropopause. Long-lived tracers are generally well-mixed in the troposphere, with moderate gradients away from surface sources for growing species [*Prather et al.*, 1987; *Plumb and McConalogue*, 1988] and a small roll-off toward the tropopause due to mixing with stratospheric air [*Tuck et al.*, 1997a]. Tracer gradients at the tropopause are therefore discontinuous in theory and poorly defined in practice. Of concern here are the gradients at the tropopause as it is approached from the lower stratosphere above. The task at hand is thus to determine the slope of a stratospheric correlation curve at its very endpoint, a straightforward matter only if the correlation is known to be strictly linear over some range above the tropopause.

While the "global mixing" model described by *Plumb and Ko* [1992] predicts a linear correlation between two species in steady state in the absence of local sources or sinks, this is not generally the case for the tropical pipe model [*Plumb*, 1996] and the more realistic "leaky pipe" model, as discussed in section 2.1. Changes in the fluxes across the tropical/midlatitude boundary are expected to result in curvature in the correlations in the respective region of the stratosphere. Apart from these deviations from linearity induced purely by transport, curvature generally results either from local sources and sinks or local growth causing vertical gradients in the global fluxes. For the tracers considered here, local chemistry should be a factor in the vicinity of the tropopause only for H-1211. The dominant factor causing curvature in correlation diagrams for most species is likely to be tropospheric growth. The magnitude of the curvature introduced depends on the contribution of growth to the global tracer flux through a given isopleth; that is, long-lived species are more affected than shorter-lived ones with identical growth rates. In the case of SF_6, the global flux is exclusively due to growth; therefore, correlations between long-lived tracers and SF_6 (and thus mean age) show the largest curvature. Because of the exponential decline of air density with altitude, the greatest curvature is generally introduced at the lowest altitudes, that is, just above the tropopause, which complicates the slope determination at the tropopause.

Our goal is to determine the slopes at the tropopause of the correlations of the long-lived tracers with age (Figure 6) and with CFC-11 (Figure 7). All available extratropical observations from ASHOE/MAESA are combined in these correlation diagrams, with the following exceptions. First, we exclude southern hemisphere data above Θ = 475 K in October 1994 that we believe indicate a seasonal departure from universality, as discussed in section 3.2.1. These high-altitude observations are located at the far end of the correlation diagrams and are thus of little relevance for the slopes to be determined. Second, no observations below the tropopause are included as any vertical

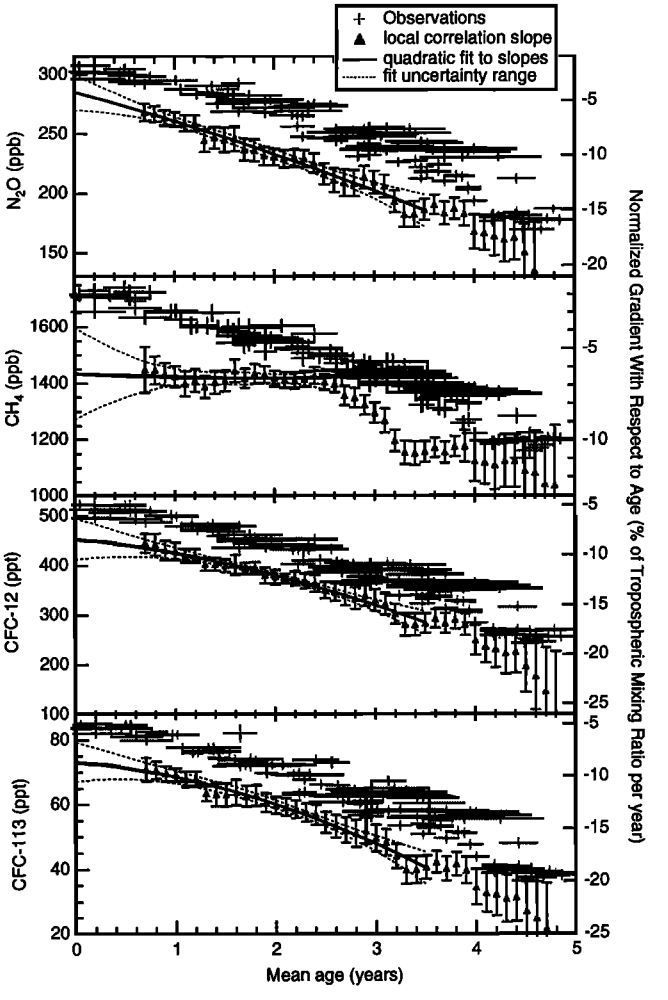

Figure 6a. Correlations between mixing ratios of long-lived tracers CFC-113, CFC-12, CH_4, and N_2O and age (left axes, plusses; symbol size indicates uncertainty), normalized local correlation slopes (triangles with error bars, right axes) and quadratic fits with uncertainty envelopes (lines, right axes). See text for details.

tracer gradients in the upper troposphere are not expected to result in smooth continuations of the stratospheric correlations; in fact, there appear to be kinks in the correlations at the tropopause if tropospheric data is included. Finally, we use observations from only the fourth deployment (October/November 1994) for CH_4, CFC-113, and CH_3CCl_3. For both CH_4 and CFC-113, instrumental performance improved drastically for the fourth deployment. Earlier data, particularly those obtained close to the tropopause during ascents and descents, are of poor precision and appear to be inconsistent with the October/November observations. A calibration gas mixture containing the measured gases at tropospheric ambient levels was flown during most of the fourth deployment (but not the other deployments) producing the most reliable data close to the troposphere during that deployment. In the case of CH_3CCl_3, data from different deployments cannot be combined because mixing ratios near the tropopause declined by more than 5% during the course of the mission due to the rapid negative growth in the troposphere (close to 10% $year^{-1}$); again, observations from the last deployment, combining both hemispheres, are the most reliable.

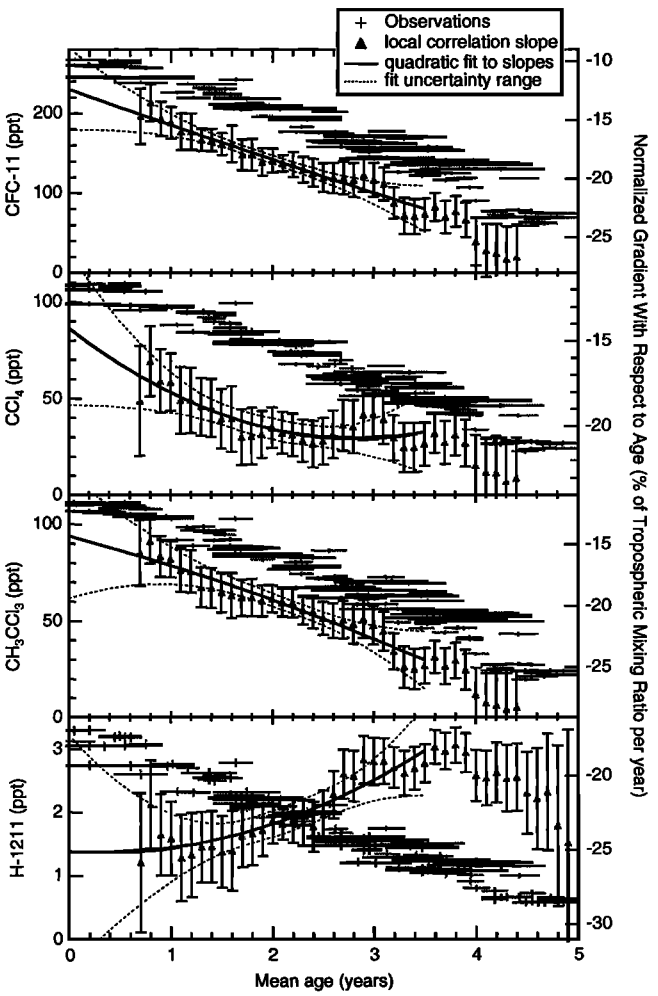

Figure 6b. Same as Figure 6a, but for H-1211, CH_3CCl_3, CCl_4, and CFC-11.

The determination of the slope of a correlation diagram at its endpoint is a difficult task once curvature occurs and the functional form of the correlation is not a priori known. When deriving the slope from an analytical curve fit to the correlation diagram, the greatest bias is introduced at the endpoints if the actual correlation does not adhere to the prescribed functional form. Nonparametric fitting and smoothing routines avoid this problem, but usually perform poorly at the endpoints if they provide endpoint values at all. These difficulties are inherent to the nature of the problem, and no approach will be completely free of bias.

Our strategy here is to address the endpoint problem in the space of the quantity of interest, that is, the slope of the correlation curve, as to not obscure bias that might occur. For each of the correlations $Y(X)$ displayed in Figures 6 and 7 we measure the slopes dY/dX at points evenly spaced along the X axis (every 0.1 years of age and every 5 ppt of CFC-11) as the slope of a local linear regression within some window (ΔX) centered on each point. The local line fits are weighted using the uncertainties of the individual observations, which are represented in Figures 6 and 7 as the size of the symbols (pluses). A fitting routine that accounts for uncertainties in both X and Y coordinates [*Press et al.*, 1992] was found essential to eliminate sensitivity of the local slope measurements to switching the X and Y axes. The width of the window (ΔX) is chosen to be large enough to average out seasonal signals and to create reasonably smooth curves of dY/dX versus X (triangles with error bars in Figures 6 and 7), but not so large as to smooth out structure of interest, resulting in widths of 2 years age and 70 ppt CFC-11 (except 100 ppt CFC-11 for the correlations of CH_4, CFC-113, and CH_3CCl_3 versus CFC-11 that incorporate a much smaller amount of observations). For values of X closer to the endpoints than $\Delta X/2$, the window width ΔX is decreased, such that the window edges ($X \pm \Delta X/2$) do not exceed the range of the observations, until the window is too narrow to constrain the slope reliably; that is, that is, slope values start to fluctuate erratically. The gap of measured slopes in Figures 6 and 7 marks the region in the vicinity of the endpoint at the tropopause (i.e., $\Gamma = 0$ and [CFC-11] = 270 ppt) where no reliable local slope can be deduced due to insufficient range of the observations.

This procedure makes the problem of slope determination at the endpoint rather transparent. While the endpoint slope itself is an unmeasurable quantity, it is certainly related to the slopes in the vicinity of the endpoint, and inferring it is essentially a matter of judicious extrapolation. Two decisions have to be made regarding the extrapolation: first, what is a reasonable range of observations that might be related to the endpoint in a simple way, and second, what is a reasonable representation of this relation. The answers must be based on the derived smooth slope

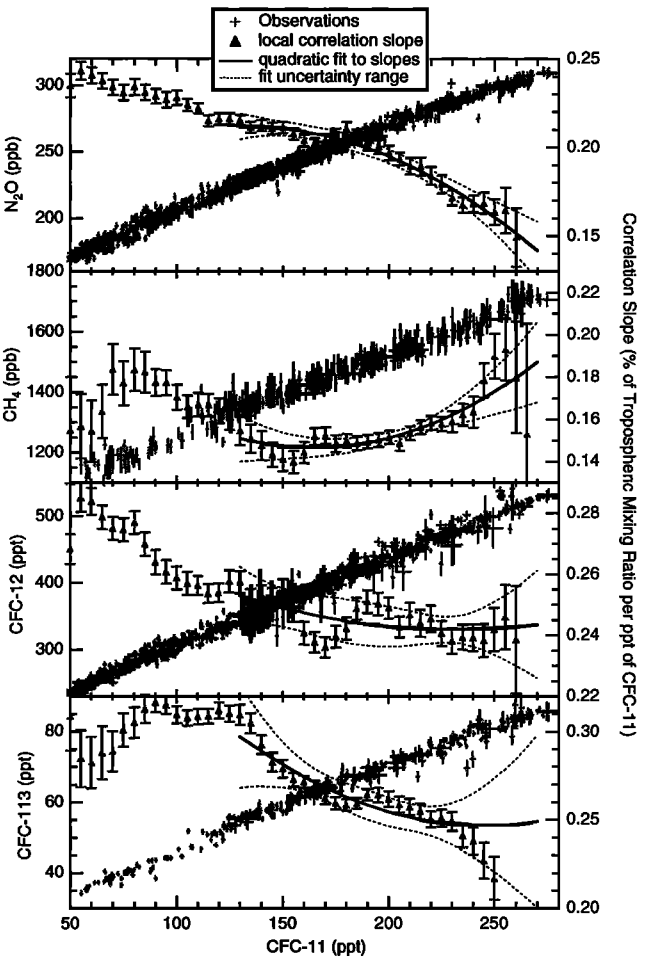

Figure 7a. Correlations between mixing ratios of long-lived tracers CFC-113, CFC-12, CH_4, and N_2O and CFC-11. Symbols and lines have identical meaning as in Figure 6.

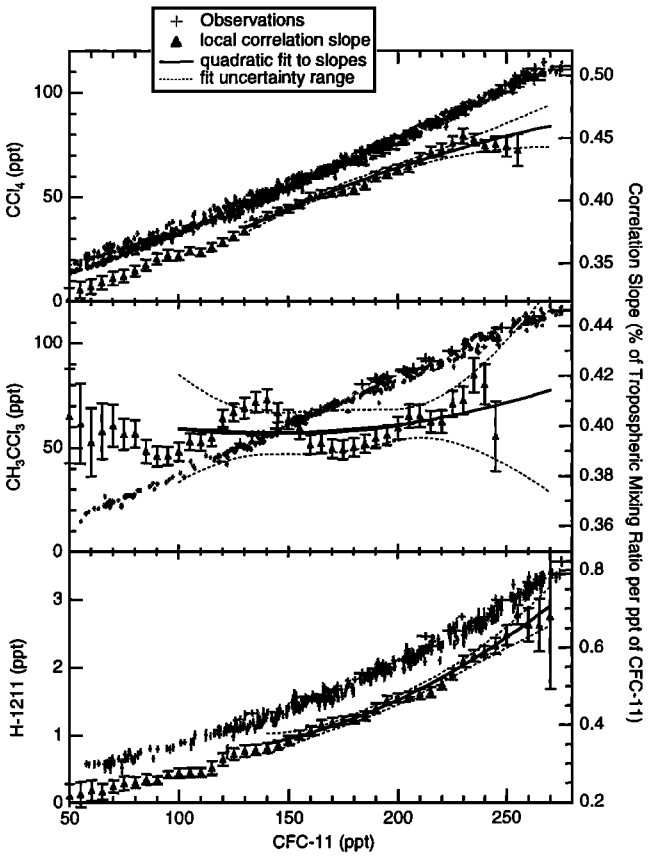

Figure 7b. Same as Figure 7a, but for H-1211, CH_3CCl_3, and CCl_4.

curves as well as on knowledge of the physical processes governing the shape of the correlations.

The relevant processes influencing the correlations' shapes in the vicinity of the tropopause are local growth and perhaps changes in the fluxes across the midlatitude/tropical boundary, as discussed above. Chemistry becomes important only at higher altitudes (except for H-1211) causing large curvature at the correlations' far end (outside the range displayed in Figures 6 and 7). The slope curves indeed exhibit increasing structure and a change in curvature for ages greater than about 4 years or CFC-11 mixing ratios smaller than about 100 ppt. This sets an upper limit to the range of observations from which a simple relation between dY/dX and X can be inferred and extrapolated to the endpoint. From a practical point of view, this range should be maximized in order to minimize the influence of noise in the slope curves that might bias the extrapolation.

The choice of the relation between dY/dX and X is guided by the following considerations. The processes (mentioned above) responsible for curvature in the correlations in the lowermost stratosphere are expected to act smoothly on timescales of a few years, apart perhaps from annual cycles that are not of interest here and were smoothed out by the large window size (2 years) over which the slopes were measured. Within the age range of interest (0 to 4 years) we do therefore not expect any structure in the slope curves higher than second order. This allows for third-order structure in the correlation curves themselves. We fit quadratic functions to the slope curves for ages up to 3.5 years (Figure 6) and CFC-11 mixing ratios corresponding to the same age range, that is, upward from 130 ppt (Figure 7); the individual slope values are weighted using their uncertainties (error bars in Figures 6 and 7) as inferred from the local linear regression. Most of the slope curves displayed in Figures 6 and 7 are indeed well described by a quadratic function over the range chosen. Much of the higher-order structure that is apparent, for example, in the slope curves of Figure 7, is systematic noise due to the nonuniform distribution of the observations in phase space and can often be recognized directly in the correlations as an outlier group of measurements. In cases where such noise created an obviously unrealistic fit curve, we slightly modified the range over which the quadratic was fit (for CH_4 versus age and CH_3CCl_3 versus CFC-11, compare Figures 6 and 7) as to average out the noise structure. In general, however, the predicted slope values at the tropopause are not particularly sensitive to the exact choice of fit range.

The uncertainties of the derived slopes at the tropopause are difficult to assess in a rigorous way as the analysis involved certain assumptions as well as subjective judgment. We estimate here only a statistical uncertainty of the extrapolated fit value at the tropopause using the bootstrap technique [*Efron and Tibshirani*, 1991], that is, by repeating each fit many (500) times with random "bootstrap" samples of identical size, drawn with replacement from the original sample of points fitted. In deriving an uncertainty from the standard deviation of the repeated fits, one has to recall that the points fitted are not all independent because each point combines information within a range (the window size ΔX) larger than the distance to its nearest neighbor. We take this redundancy into account by scaling the standard deviation of the repeated bootstrap fits by the square root of the number of points involved in each fit over the square root of completely independent points within the range of fitted values. The fit uncertainty envelopes derived in this fashion are displayed in Figures 6 and 7.

The slopes at the tropopause (in absolute units) and their uncertainties as inferred from Figures 6 and 7 are given in Table 1. On the basis of this analysis, the slopes at the tropopause can be constrained to within 10% or better (except 20% for CFC-113) for the correlations of long-lived tracers versus CFC-11, and to within 20 to 40% for the correlations of long-lived tracers versus age. Note that in the latter case the systematic error due to the uncertainty of Λ in the age calculation (compare equation (21) and Figure 5) is small (~2%) and was neglected in the uncertainty estimate. The large uncertainties in this case are due to the larger curvature in the correlations with age as well as the small number of age observations close to the tropopause obtained during ASHOE/MAESA.

Table 1. Correlation Slopes at the Tropopause Inferred From Figures 6 and 7

	$d\chi/d\Gamma$, ppt yr^{-1}	Uncertainty, %	$d\chi/d\chi_{CFC\text{-}11}$, ppt/ppt	Uncertainty, %
N_2O	-13,000	38	436	11
CH_4	-109,000	40	3230	10
CFC-12	-43.8	25	1.29	7
CFC-113	-7.3	22	0.212	20
CFC-11	-33.5	28	(1)	–
CCl_4	-15.9	32	0.515	3.6
CH_3CCl_3	-16.3	35	0.472	10
H-1211	-0.84	31	0.0237	7

4.3. Correction for Tracer Transience

For a tracer that is not in steady state in the atmosphere, the flux through the tropopause is balanced by the integrated sink plus the accumulation rate above the tropopause. The relation between stratospheric lifetime τ and the tracer gradient at the extratropical tropopause following from (13) is thus

$$\frac{B}{\tau}+\frac{\partial B_u}{\partial t}=-\left.\frac{d\chi}{d\Gamma}\right|_{\chi_0} M_u \qquad (22)$$

where B_u is the burden of the species above the tropopause. For the species under consideration, $B_u \approx 0.1B$. Thus it is easily seen that the relative contribution of the growth term is of the order of 0.1τ times the relative growth rate (averaged over several years prior to the observation time). If the lifetime is 100 years, then neglecting a steady growth of only 1% year^{-1} will cause a ~10% error in the derived lifetime. The tracers considered here have exhibited growth rates of several percent per year in recent years, with the exception of N_2O and CH_4 which have grown with rates about a factor of 5 smaller than that. Growth therefore cannot be neglected.

The calculation of the growth term in (22) is difficult unless the tropospheric growth has been steady and nearly linear for at least several years such that it can be assumed that mixing ratios everywhere above the tropopause are growing at the same rate. This condition is not met for the tracers under consideration. In fact, the tropospheric growth rates for the CFCs started their decline from several percent per year to nearly 0 in the 6 years prior to 1994 [*Elkins et al.*, 1993; *Montzka et al.*, 1996], while CH_3CCl_3 and CCl_4 concentrations leveled off earlier and have already declined for a number of years [*Prinn et al.*, 1995; *Montzka et al.*, 1996]. Under these circumstances, the only hope of calculating the total stratospheric accumulation rate would be to approximate the growth rate at a particular location in the stratosphere with the tropospheric growth rate at the mean time of stratospheric entry of the air at that location. Even this approximation would require knowledge of the global distribution of mean age. Calculation of the growth term is therefore generally feasible only with the help of a global transport model.

We also note that the term B/τ in (22) represents the instantaneous sink above the tropopause which generally differs from the sink in equilibrium. The term τ in (22) thus represents the instantaneous (or "transient") lifetime rather than the steady state lifetime. The transient lifetime is a less useful quantity for comparison with model calculations as it depends on the time dependent boundary condition (e.g., emission history of the gas) and the detailed time response of the model in question [cf. *Kaye et al.*, 1994, p. 5-8].

Because of these difficulties in using (22) to derive lifetimes, we will pursue a different approach of accounting for a tracer's growth, namely using the tropospheric time series and the age of the air to derive steady state gradients $d\sigma/d\Gamma$ at the tropopause from the observed nonsteady state gradients $d\chi/d\Gamma$, and then apply the equations valid for steady state tracers, (3) and (14), to derive steady state lifetimes. The simplest approach of relating the observed mixing ratios (χ) to those representative of a steady state situation (σ) would be to assume that the mixing ratio of a long-lived tracer in an air parcel at location $\mathbf{x}$ in the stratosphere is always proportional to the mixing ratio at the time of stratospheric entry of this air parcel, or more correctly (recalling that air parcels contain a mixture of air of different entry times), proportional to a mean mixing ratio of stratospheric entry given by

$$\chi_{\text{entry}}(\mathbf{x},t)\equiv\int_0^\infty \chi_0(t-t')G(\mathbf{x},t')dt' \qquad (23)$$

where the symbols have the same meaning as earlier. If this assumption holds, stratospheric mixing ratios $\sigma(\mathbf{x})$ corresponding to a steady state with tropopause mixing ratio σ_0 can be readily derived from

$$\frac{\sigma(\mathbf{x})}{\sigma_0}=\frac{\chi(\mathbf{x},t)}{\chi_{\text{entry}}(\mathbf{x},t)}\,. \qquad (24)$$

In the appendix we investigate in detail the nature of the relation between stratospheric steady state and transient mixing ratios in the vicinity of the tropopause and show that this simple scaling approach is inappropriate for all but the longest-lived of the species considered here and cannot generally be used to derive steady state slopes needed for the lifetime calculation. Instead, we derive a relation between the observed gradients with respect to age at the tropopause ($d\chi/d\Gamma$) and the gradients $d\sigma/d\Gamma$ corresponding to a steady state situation with the same tropopause mixing ratio as the one observed (i.e., for $\sigma_0=\chi_0(t)$, t being October 1994):

$$\left.\frac{d\sigma}{d\Gamma}\right|_{\Gamma=0}=\left(\left.\frac{d\chi}{d\Gamma}\right|_{\Gamma=0}+\gamma_0\sigma_0\right)\Big/\left(1-2\gamma_0\Lambda\right) \qquad (25)$$

where Λ is, as defined in (20), a measure for the width of the age spectrum (Δ) and γ_0 is the effective linear growth rate of the tracer, meaning that tropospheric linear growth at rate γ_0 would create the same gradient $d\chi/d\Gamma$ at the tropopause as the true (possibly nonlinear) growth that the tracer experienced prior to the time of the observations. The presence of Λ in (25) accounts for the fact that, due to the finite width of the age spectrum, the contributions of tropospheric growth and of chemical sinks to the overall tracer gradient at the tropopause are mutually dependent; the simper scaling approach of (24) ignores this dependence (compare the appendix for details). Λ again has to be obtained from three-dimensional transport models; as earlier, we adopt a value of 1.25 ± 0.5 years (compare section 4.1). In the appendix it is shown that for a quadratic tropospheric time series of the form

$$\chi_0(t')=\chi_0(t)\cdot\left[1+b\cdot(t'-t)+c\cdot(t'-t)^2\right] \qquad (26)$$

it is $\gamma_0=b-2\Lambda c$.

The tropospheric time series of most any long-lived species can be approximated very well by a quadratic function over a time interval of several years. The relevant time interval over which expansion (26) needs to be a good approximation is given by the time interval spanned by the age spectrum at the tropopause, $G(0,t')$. Although the spectral width is small at the tropopause (about 1 year, according to equation (20)), one has to recall that the age spectrum has a long tail such that long transit times contribute to the age distribution even at the tropopause.

We therefore fit quadratic functions to the global surface time series over a 5-year interval prior to mid-1994 and then derive the growth coefficients b and c for the expansion (26) about $t = 1994.0$ (instead 1994.8, to take into account the 0.8 year delay between the global mean surface values and the tropopause).

Global monthly surface means over the relevant time interval were obtained from a number of sources: For N_2O, CH_4, CFC-12, CFC-11, CCl_4, and H-1211 we use in situ and flask data from the NOAA/CMDL global network of monitoring stations [*Elkins et al.*, 1996b; *Tans et al.*, 1996]; methods are described, and much of these data are presented by *Elkins et al.* [1993] and *Montzka et al.* [1996] for the CFCs, *Butler et al.* [1992, 1997] for H-1211, and *Dlugokencky et al.* [1994] for CH_4. For CFC-113 and CH_3CCl_3, for which the NOAA/CMDL data record does not reach back far enough in time, we derived global surface means using data from the Atmospheric Lifetime Experiment/Global Atmospheric Gases Experiment (ALE/GAGE) network [*Prinn et al.*, 1995; *Fraser et al.*, 1996]. Note that differences in the absolute calibrations between the two networks and the ACATS-IV data are irrelevant for the growth correction because only relative growth rates enter in (25). The linear and quadratic relative growth rates b and c derived from these global time series are listed in Table 2, along with their uncertainties and the resulting effective linear growth rate $\gamma_0 = b - c \times 2.5$ years.

The normalized steady state gradients $\beta_0 \equiv -(d\sigma/d\Gamma)/\sigma_0$, as derived from the observed gradients $d\chi/d\Gamma$ by means of (25), are also listed in Table 2, along with their uncertainties. The uncertainties were calculated from the uncertainties of the observed slopes (compare Table 1), the uncertainties of the growth coefficients given in Table 2, and an assumed uncertainty of 0.5 years for Λ. Finally, Table 2 lists the correction factor C and its uncertainty, C being defined as

$$C \equiv \left(\frac{d\sigma}{d\Gamma} \Big/ \frac{d\chi}{d\Gamma} \right)_{\Gamma=0} \tag{27}$$

The uncertainties of the correction factors are due mainly to the large uncertainty of the spectral width Δ (taken into account by the uncertainty of Λ) that determines the contribution of the quadratic growth rate c to the effective linear growth rate γ_0 ($=b-2\Lambda c$) and also determines (via equation (25)) the contribution of growth to the overall tracer gradient for a given γ_0. The correction factors are thus most poorly constrained for the tracers with the largest nonlinear growth rates c (CFC-113, CH_3CCl_3) and generally less well constrained for the shorter-lived tracers for which the growth contribution to the overall tracer gradient depends more heavily on the width of the age spectrum.

The uncertainty in the steady state gradient β_0 is mostly dominated by the uncertainty of the observed gradients with respect to age (Table 1) that is generally larger than the correction for transience itself (except for CFC-113). This is not true, however, for the slopes with respect to CFC-11 obtained from Figure 7 that are much better constrained. The steady state slopes with respect to CFC-11 are readily obtained using the correction factors from Table 2:

$$\frac{d\sigma_i}{d\sigma_{\text{CFC-11}}} = \frac{d\chi_i}{d\chi_{\text{CFC-11}}} \frac{C_i}{C_{\text{CFC-11}}} \tag{28}$$

4.4. Global Burden Calculation

The slopes derived in the previous sections provide information about the integrated stratospheric sinks. To calculate stratospheric lifetimes, global burdens need to be known (equations (3) and (14)). Because 80% of the atmospheric mass resides in the troposphere, the ratio of global burdens of two long-lived tracers in (3) may be roughly (to within ~10%) approximated by the ratio of their tropospheric mixing ratios, as suggested by *Plumb and Ko* [1992]. This approximation is particularly useful if the species' mixing ratios decline at similar rates in the stratosphere. For the sake of the highest accuracy and since we require the absolute burdens in (14), we will here explicitly calculate global burdens, corresponding to a steady state with tropospheric mixing ratios as observed in October 1994.

We calculate the global burden of a species as

$$B = \int_{\text{atmosphere}} \rho \sigma d^3\mathbf{x} = M_a \bar{\sigma} \tag{29}$$

where $M_a = 5.132 \times 10^{18}$ kg is the dry air mass of the atmosphere [*Trenberth and Guillemot*, 1994], and a mass weighted atmospheric average mixing ratio is defined as

$$\bar{\sigma} \equiv \frac{1}{p_S} \int_0^{\pi/2} \int_0^{p_S} \sigma \cos\phi \, dp d\phi \tag{30}$$

where p is pressure, the mean surface pressure $p_S = 982.4$ mbar [*Trenberth and Guillemot*, 1994], ϕ is latitude, and where the mixing ratio is assumed to be zonally symmetric and meridionally symmetric about the equator everywhere.

We divide the hemisphere into four latitude bands: tropics (0 to 25°), midlatitudes (25° to 50°), high latitudes (50° to 70°), and polar latitudes (70° to 90°), and construct mean vertical profiles

Table 2. Linear (b), Quadratic (c), and Effective Linear (γ_0) Growth Rates, Derived Normalized Steady State Gradient (β_0) With Respect to Γ, and Correction Factor C

	b, % Year^{-1}	c, Year^{-2}	γ_0, % Year^{-1}	β_0, % Year^{-1}	$\delta\beta_0/\beta_0$, (%)	C
N_2O	0.10 ± 0.02	-0.024 ± 0.005	0.16	4.07	39	0.97 ± 0.02
CH_4	0.11 ± 0.04	-0.081 ± 0.009	0.31	6.04	42	0.96 ± 0.02
CFC-12	1.9 ± 0.1	-0.13 ± 0.03	2.23	6.41	25	0.77 ± 0.07
CFC-113	1.4 ± 0.4	-0.86 ± 0.04	3.51	5.53	39	0.65 ± 0.12
CFC-11	-0.11 ± 0.08	-0.32 ± 0.02	0.69	11.9	30	0.96 ± 0.02
CCl_4	-0.68 ± 0.09	-0.029 ± 0.002	-0.61	14.6	30	1.03 ± 0.02
CH_3CCl_3	-7.5 ± 0.46	-1.61 ± 0.08	-3.5	16.4	30	1.14 ± 0.13
H-1211	5.7 ± 0.24	0	5.7	22.6	41	0.90 ± 0.10

for each band combining a variety of observations. Mixing ratios in the troposphere below 400 mbar are set equal to the global mean surface mixing ratios observed by the NOAA/CMDL network of global monitoring stations in October 1994 [*Montzka et al.*, 1996; *Butler et al.*, 1997; *Tans et al.*, 1996]. Our strategy for higher altitudes is to first construct vertical profiles for N_2O and then use stratospheric correlations to derive vertical profiles for the other species.

The ER-2 N_2O measurements obtained by ATLAS during ASHOE/MAESA reach up to 50 mbar and span all but the polar latitudes. The ATLAS measurements are consistent with the NOAA/CMDL mean surface value of 311 ppb and agree well with the ACATS-IV N_2O measurements in October 1994 that are intercalibrated with the surface measurements. More than 95% of the atmospheric burden of N_2O can thus be consistently accounted for with surface and aircraft observations. For the uncovered polar latitudes and higher altitudes we complement this database with observations from the following sources: ground-based millimeter wave spectroscopic measurements up to 45 km over the south pole in March and October 1993 [*Crewell et al.*, 1995]; balloon-borne cryogenic samples obtained up to 28 km at 68°N in February 1987 and 1988 [*Schmidt et al.*, 1989]; and spaceborne measurements up to 62 km between 3.4°N and 49.2°N obtained from the Atmospheric Trace Molecule Spectroscopy (ATMOS) experiment on the space shuttle in November 1994 [*Gunson et al.*, 1996]. We scaled the pre-1994 observations to a tropospheric mixing ratio of 311 ppb. Questions about the consistency of the different data sets with the ATLAS data are of little concern here because of the small amount of N_2O mass covered by these observations. We divided all observations into the four latitude bands, averaged them into 2-km bins, and derived vertical profiles in each band by fitting smooth splines that merged to 311 ppb at 400 mbar and to 0 ppb at 0 mbar (Figure 8a).

Stratospheric profiles for all the other species are then constructed using tracer-tracer correlations as follows. Stratospheric profiles in all four latitude bands for CFC-12 and CFC-113, which have similar lifetimes and chemical sinks as N_2O, are based on the extratropical correlation with N_2O observed during ASHOE/MAESA. CH_4 and CFC-11 show different correlations with N_2O in the tropics [*Michelsen et al.*, 1995; *Volk et al.*, 1996]; thus we separate the data into tropical and extratropical regions, and derive tropical vertical profiles from the tropical correlation, profiles for all other latitudes from the extratropical correlation. Because the tropical range of N_2O mixing ratios as well as the overall range of CH_4 mixing ratios sampled by the ER-2 is rather small, we supplement with ATMOS data of CH_4 and CFC-11 to define the correlations over their full range (Figures 8b and 8c). Profiles for the remaining, shorter-lived species CCl_4, CH_3CCl_3, and H-1211 are based on the extratropical correlation with CFC-11, except for the tropical H-1211 profile that is based on the tropical correlation. The profiles were obtained by fitting smooth splines like the ones shown in Figures 8b and 8c.

In general, the upper tropospheric ACATS-IV observations during the fourth deployment agree to within 1-2% with the observed global surface means for October 1994, as is expected since all NOAA/CMDL measurements are tied to the same gravimetric standards. The derived stratospheric profiles can thus be merged with the assumed tropospheric ones at 400 mbar, analogous to the N_2O profiles. Two species, however, show significant discrepancies. CCl_4 and H-1211 mixing ratios in the upper troposphere are consistently about 9% higher than the October surface means of 103 ppt [*Montzka et al.*, 1996] and 3.1 ppt [*Butler et al.*, 1997], respectively. Although the absolute calibration scale of the measurements is irrelevant for the lifetime calculation, the calculation of the global burdens must be consistent with the stratospheric measurements used to derive the correlation slopes. For the purpose of the global burden calculation, we simply scale the stratospheric profiles of CCl_4 and H-1211 to match the surface values in the upper troposphere such that the derived average atmospheric mixing ratios, $\bar{\sigma}$, are consistent with the global mean surface values.

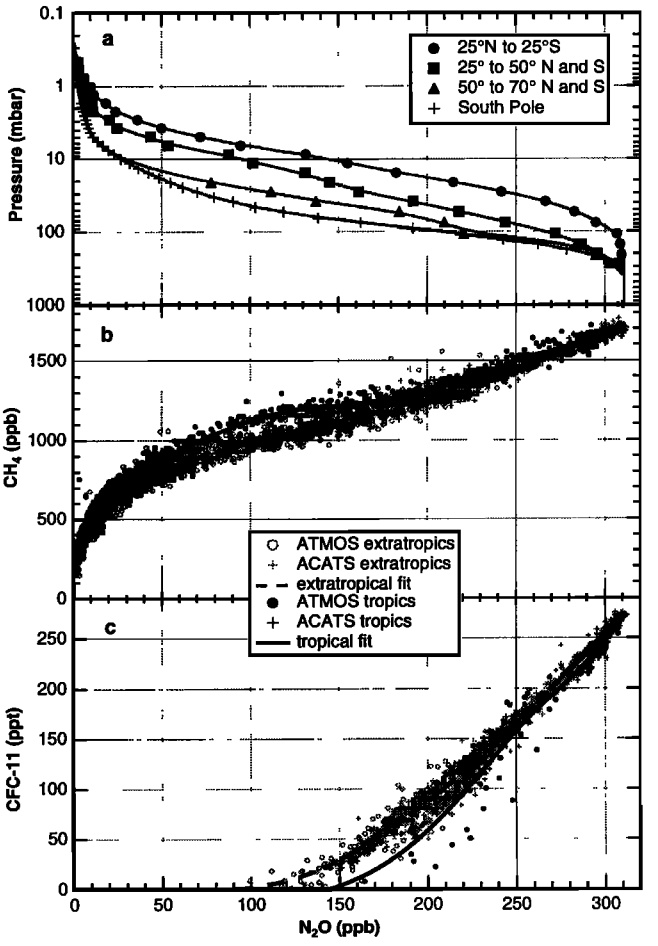

Figure 8. (a) Stratospheric vertical profiles of N_2O for different latitude bands derived from ATLAS ER-2 observations during ASHOE/MAESA, ATMOS spaceborne observations, and other sources as described in text. Correlations of (b) CH_4 and (c) CFC-11 with N_2O mixing ratios from ER-2 and ATMOS observations as used to construct stratospheric vertical profiles for these species.

If the discrepancies between aircraft and surface measurements merely reflect differences in their absolute calibration scales, then the correlation slopes for CCl_4 and H-1211 derived in section 4.2 now have to be rescaled by the same amount (0.91) for use in the lifetime calculation. However, the standard mixtures flown during ASHOE/MAESA are nominally based on the same calibration scale as the NOAA/CMDL surface measurements. This is of concern, since the discrepancies may then be an indication of an unknown systematic error in the ACATS-IV measurements, for example, coelution in the chromatograms of unidentified long-lived species

present in stratospheric air or contamination in the air inlet (contamination within the instrument can be excluded since it is diagnosed by periodic blank air injections). If such an error caused a nearly constant positive offset of 9% of the measurements, it would not change the correlation slopes and scaling them would be inappropriate. At this point, neither a proportional error due to calibration errors nor an offset due to instrumental errors can be excluded, but we can assert that the true correlation slopes (i.e., the ones consistent with the global burdens calculated here) for CCl_4 and H-1211 fall between 91 and 100% of the observed ones. For the lifetime calculation, we thus opt to scale the slopes by 0.955 and add to them systematic uncertainties of 4.5%.

The average atmospheric mixing ratios $\bar{\sigma}$ calculated according to (30) are given in Table 3, along with the corresponding global mean surface mixing ratios σ_S used in the calculation. One might expect that the major uncertainty in the calculation stems from assigning global mean surface mixing ratios uniformly to the lower 60% of the atmospheric mass. Spatial variability can be substantial in the lower troposphere for long-lived tracers exhibiting substantial growth, in particular if surface sources are nonuniformly distributed [*Prather et al.*, 1987; *Plumb and McConalogue*, 1988]. Note, however, that our goal was to calculate average atmospheric mixing ratios representative for a steady state situation, in which case the troposphere would be indeed well mixed.

The accuracy of the calculation is then determined by how consistent the assumed tropospheric mixing ratios are with the stratospheric observations used to derive the correlation slopes. Considering the good agreement between the upper tropospheric observations and the global surface means, we estimate this uncertainty as 2%. We estimate that the stratospheric contribution to the global burdens (which is only of the order of 10%) was accounted for to better than 10%, such that it does not contribute substantially to the total uncertainty of the average atmospheric mixing ratios.

5. Results and Discussion

We finally calculate stratospheric lifetimes and lifetimes relative to the CFC-11 lifetime based on (3) and (14) and the results from previous sections as

$$\tau = -\bar{\sigma} M_a \Big/ \left(M_u C \frac{d\chi}{d\Gamma}\Big|_{\Gamma=0} \right) \tag{31}$$

Table 3. Global Mean Surface and Average Atmospheric Mixing Ratios in October 1994

	σ_s	$\bar{\sigma}$
N_2O, ppb	311	297
CH_4, ppb	1725	1670
CFC-12, ppt	528	500
CFC-113, ppt	84.5	79.8
CFC-11, ppt	272	251
CCl_4, ppt	103.1	94.6
CH_3CCl_3, ppt	116	106.6
H-1211, ppt	3.1	2.8

and

$$\tau = \tau_{\text{CFC-11}} \cdot \frac{\bar{\sigma}}{\bar{\sigma}_{\text{CFC-11}}} \Big/ \left(\frac{C}{C_{\text{CFC-11}}} \frac{d\chi}{d\chi_{\text{CFC-11}}}\Big|_{[\text{CFC-11}]=270\,\text{ppt}} \right) \tag{32}$$

where the correction factors C are given in Table 2, the average mixing ratios are given in Table 3, the slopes at the tropopause are the ones listed in Table 1 (scaled by 0.955 for CCl_4 and H-1211, as explained earlier), and the dry air mass is $M_a = 5.132 \times 10^{18}$ kg.

The mass above the tropopause, M_u, introduces an additional uncertainty in the lifetime calculation of (31). Since most of the mass of the upper atmosphere lies close to the tropopause, M_u is dependent on the particular definition of the tropopause used. In a recent detailed calculation based on global meteorological analysis, *Appenzeller et al.* [1996] define the tropopause by the 380 K isentrope in the tropics and the 2 potential vorticity unit (PVU = 10^{-6} K m^2 s^{-1} kg^{-1}) surface in the extratropics and obtain an annually averaged stratospheric mass of $M_u \approx 11 \times 10^{17}$ kg, some 20% higher than (less rigorous) estimates based on the conventional "thermal" definitions of the tropopause [e.g., *Warneck*, 1988], which involve the lapse rate or the temperature minimum. Some of the discrepancy stems from the fact that the 2 PVU surface in the extratropics generally lies below the tropopause defined by the conventional criteria [*Hoerling et al.*, 1991; C. Appenzeller, personal communication, 1996]. This raises the question of which definition of the tropopause best approximates the control surface relevant for the lifetime calculation in (31), that is, the $\Gamma = 0$ surface or $[SF_6] = 3$ ppt isopleth at which the gradients were determined. The distinction between stratospheric and tropospheric observations in this work is based mainly on the minimum temperature in the vertical profiles measured by the ER-2, with use of H_2O, and N_2O profiles for verification. These tropopause heights lie generally above the 2 PVU surface (mostly between 2 and 5 PVU) in the extratropics; indeed, all of the extratropical upper tropospheric measurements of SF_6 that contributed to the reference value of 3 ppt for $\Gamma = 0$ lie above the 2 PVU surface. We therefore believe that the 3 PVU surface is a more suitable approximation for the $[SF_6] = 3$ ppt isopleth in the extratropics. A calculation analogous to the one of *Appenzeller et al.* [1996], but using the extratropical 3 PVU surface as lower bound, yields $M_u = 9.8 \times 10^{17}$ kg in the 2-year (1992-1993) average (C. Appenzeller, personal communication, 1996). We attribute an uncertainty of 10% to this value, which is about 12% lower than the stratospheric mass calculated by *Appenzeller et al.* [1996], but 10-15% higher than estimates used in earlier literature [*Reiter*, 1975; *Murgatroyd and O'Neill*, 1980].

Table 4 summarizes the results and their uncertainties (1 s.d.), derived from the uncertainties of all inputs, as discussed in the previous sections. For the lifetime estimates based on the correlations with CFC-11, the uncertainty of the CFC-11 lifetime is not included in Table 4. The stratospheric steady state lifetimes derived here are equal to atmospheric lifetimes for all species but CH_4, CH_3CCl_3, and H-1211. Also listed in Table 4 are the lifetime values used in recent IPCC and WMO reports. The lifetimes recommended in *WMO* [1995] were derived as the average of the results from the reporting 2-D models in *Kaye et al.* [1994], scaled

Table 4. Stratospheric Steady State Lifetimes From This Analysis Compared to Current Recommended Values and Model Results

	Based on Correlation With Age	Based on $\tau_{CFC\text{-}11}$ = 41 Years[a]	Based on $\tau_{CFC\text{-}11}$ = 50 Years[a]	WMO/IPCC Values	Model Range[b]
N_2O	124 ± 49	110 ± 13	135 ± 16	120[c]	120-139
CH_4	84 ± 35	84 ± 9	103 ± 11	120[d]	–
CFC-12	77 ± 26	79 ± 10	96 ± 12	102[c]	100-123
CFC-113	89 ± 35	91 ± 25	112 ± 31	85[c]	76-96
CFC-11	41 ± 12	(41)	(50)	50[c]	40-60
CCl_4	32 ± 11	29 ± 3	36 ± 4	42[c]	30-53
CH_3CCl_3	30 ± 9	31 ± 5	38 ± 6	45[d]	–
H-1211	20 ± 9	21 ± 4	26 ± 5	36[e]	–

Steady state lifetimes are in years.

[a] Uncertainty of CFC-11 lifetime not included in uncertainty estimate.

[b] *Kaye et al.* [1994, Table 5.3].

[c] *WMO* [1995, Table 13-1].

[d] *IPCC* [1995, Table 2.2].

[e] *WMO* [1992, Table 6.2, scaled to $\tau_{CFC\text{-}11}$= 50 years].

to a CFC-11 lifetime of 50 years. The ranges of these model results as given in *Kaye et al.* [1994] are listed in Table 4 as well.

The uncertainties of our lifetime estimates based on the correlation with age are dominated by the uncertainties of the observed gradients at the tropopause and, for CFC-113, the uncertainty of the growth correction. For the lifetimes relative to the CFC-11 lifetime, the uncertainty of the correlation slope is a major contributor to the total uncertainty for all species, with equally large contributions from the uncertainty of the growth correction for CFC-12, CFC-113, CH_3CCl_3, and H-1211.

Comparison of the first two columns of Table 4 shows that the lifetimes derived from the correlations with age are consistent with the ones derived from the correlations with CFC-11 for a CFC-11 lifetime of 41 years (the value derived by the former method). Considering the different nature of the correlations displayed in Figures 6 and 7, this lends credibility to our method of deriving the correlation slopes at the tropopause and estimating their uncertainties.

Our estimate for the CFC-11 steady state lifetime of 41 ± 12 years falls at the lower end of the range calculated by current 2-D models (Table 4) and agrees well with a recent calculation based on global observations and calculated removal rates, 41.5 years (±30%) [*Minschwaner et al.*, 1993]. Our result is also in good agreement with recent inverse estimates based on global tropospheric concentrations, trends, and release inventories, yielding (depending on the specific method and model parameters used) 44^{+17}_{-10} years [*Cunnold et al.*, 1994], 52^{+23}_{-12} years, or 47^{+10}_{-7} years [*Cunnold et al.*, 1997]. Estimates from a number of inverse methods are also described by *Kaye et al.* [1994, Table 3.5.1], averaging to a steady state lifetime of 42^{+7}_{-5} years. Note that the inverse estimates obtained by *Elkins et al.* [1993] (55^{+8}_{-9} years) and *Fisher and Midgley* [1994] (56.1 years) represent transient lifetimes in (approximately) 1985, which are about 10% higher than steady state lifetimes [cf. *Cunnold et al.*, 1994, Table 8]. The currently recommended WMO value of 50 years [*WMO*, 1995] seems to be based mainly on the 2-D model results, but falls within the uncertainty range for estimates from all these different methods, including ours.

Recent inverse estimates for the steady state lifetime of CFC-12, 180^{+820}_{-81} years [*Cunnold et al.*, 1994], 122^{+91}_{-37} years [*Kaye et al.*, 1994], 172^{+416}_{-71} or 135^{+69}_{-32} years [*Cunnold et al.*, 1997], tend to be higher than estimates from 2-D models and the calculation of *Minschwaner et al.* [1993] (102 years ± 30%). Our absolute CFC-12 lifetime, that is, the one derived from the correlation with age (77 ± 26 years) is even shorter, although it agrees with the model calculations within its uncertainty. For CFC-113, our absolute result falls well within the range of 2-D model estimates, while our absolute results for N_2O and CCl_4 fall at the lower end of the model range.

Because of the limited observation set of SF_6 available for this analysis, our estimates of lifetimes relative to a given CFC-11 lifetime are considerably more accurate than the absolute lifetimes. Since the lifetimes recommended by *WMO* [1995] are scaled to a CFC-11 lifetime of 50 years, they should be compared to our results based on this CFC-11 lifetime (Table 4). The WMO values fall within the uncertainty range of our relative lifetime values for N_2O, CFC-12, and CFC-113. However, our derived relative lifetimes for CCl_4 and H-1211 are significantly (15 and 28%) shorter than the WMO-recommended values. We also derive significantly shorter stratospheric lifetimes for CH_3CCl_3 and CH_4 than the ones assumed by *IPCC* [1995]. Stratospheric removal of these two species is partly, and in the case of CH_4 predominantly, due to reaction with OH, which makes calculation of their stratospheric sinks by models more complex (and thus more uncertain) than for the other species that are predominantly lost by photolysis.

Our lifetime for CFC-113 derived from either method is longer (albeit not significantly) than the one obtained for CFC-12, contrary to all model predictions. We believe this discrepancy likely reflects the limits of our ability to accurately correct for the large and highly nonlinear growth of CFC-113 in the years prior to 1994 (compare Table 2). The nonlinearity of the growth (~15% year^{-1} in 1989 declining to essentially 0 in 1994) results in a strong dependence of the correction factor C (=0.65) on the spectral width of the age spectrum, that is, the assumed value for Λ (compare section 4.3). This dependence is, of course, also responsible for the large uncertainties of our lifetime estimates for CFC-113.

Finally, we emphasize that in deriving the age of the air (section 4.1) from SF_6 measurements we have assumed that the stratospheric vertical decline of SF_6 is driven purely by its tropospheric growth. If the influence of photochemical sinks of SF_6 is nonnegligible compared to growth, the true age of the air, and hence lifetimes based on the correlation with age, would be shorter than derived here. Considering our lifetimes are mostly already shorter than calculated by other methods, this analysis is

consistent with chemical sinks of SF_6 slow enough as to not contribute significantly to the vertical decline of SF_6 in the lower stratosphere, that is, with a SF_6 lifetime much longer than the one for N_2O. The methods developed here, however, cannot be used to actually derive a lifetime for SF_6 since it was assumed in deriving the age of the air that SF_6 is a completely conserved tracer. Use of this age in the growth correction formalism will thus necessarily return an infinite lifetime for SF_6. We note that applying (3) to SF_6 without growth correction altogether, as *Patra et al.* [1997] do (using N_2O as a reference tracer), yields not a chemical lifetime for SF_6, but a measure for its growth timescale (which is ~15 years); the reason for the long "lifetime" (1937 years) obtained in the above study is that the correlation slope was not measured at the extratropical tropopause, but in the tropical middle stratosphere. In general, the correlation slope methods described here are suitable for lifetime determination only for those tracers whose decline is predominantly caused by chemical sinks, such that the contribution to the correlation slope due to growth (to be corrected for) does not exceed that due to chemical sinks.

6. Conclusions

The methods described here offer an independent semiempirical approach for determining lifetimes of tropospheric source gases, based directly on observed abundances. We have analyzed extratropical stratospheric observations of CH_4, CFC-12, CFC-113, CFC-11, CCl_4, CH_3CCl_3, H-1211, and SF_6 (measured by ACATS-IV) and of N_2O (measured by the ATLAS instrument on board the ER-2) to derive stratospheric lifetimes for these species (excluding SF_6). The stratospheric lifetime determines the rate at which a source gas releases ozone-depleting chemicals in the stratosphere. In addition, for species lacking tropospheric loss mechanisms (all the above except CH_4, CH_3CCl_3, and H-1211), the stratospheric lifetime equals the atmospheric lifetime that determines species abundances for a given release history.

The semiempirical approach employed here is based on theoretical concepts predicting a relation between extratropical correlation slopes and global stratospheric sinks, provided the tracers in question are universally correlated at and just above the extratropical tropopause. The extensive observations during ASHOE/MAESA make it possible for the first time to investigate the validity of this assumption. The observed extratropical tracer abundances indeed exhibit compact mutual correlations that show little interhemispheric difference or seasonal variability except at higher altitudes in the southern hemisphere spring.

We have used two methods to infer stratospheric lifetimes from the observations. In the first method (SF_6-based) absolute stratospheric lifetimes are derived from the observed gradients of the species' mixing ratios with respect to mean age at the extratropical tropopause. The mean age of the air is calculated from the ACATS-IV SF_6 measurements and the tropospheric time series of SF_6, correcting for nonlinearity of the latter with use of model-derived estimates of the width of the stratospheric age spectrum. In the second method (CFC-11-based), stratospheric lifetimes relative to the CFC-11 lifetime are derived from the slopes of the tracer's correlations with CFC-11 at the extratropical tropopause. The correlations considered here generally deviate significantly from linearity in the lowermost extratropical stratosphere, due to a combination of tropospheric growth, changes in the fluxes across the midlatitude/tropical boundary, and (in the case of H-1211) local chemistry. The nonlinearity of the correlations means that highly resolved measurements in the vicinity of the tropopause are required in order to accurately determine the correlation slopes at the tropopause. The use of a lower stratospheric average slope in the lifetime determination [*Lee et al.*, 1995] would, for example, in the case of the N_2O versus CFC-11 correlation, result in an error of about 25% (compare Figure 7a) in the derived lifetime.

Because the correlation methods apply directly only to tracers in steady state, we have developed a correction for tropospheric growth involving the observed global tropospheric tracer abundances during the 5 years preceding the stratospheric measurements, the observed mean age of the stratospheric air, and the width of the stratospheric age spectrum, again estimated with the help of models. While this correction in principle can accommodate nonlinear tropospheric growth (up to second order), it may severely limit the accuracy of the lifetime determination if the growth is rapid or highly nonlinear (over the relevant stratospheric timescale of about 5 years). This is evidenced here by the large uncertainty, and likely, positive bias, in our estimates for the CFC-113 lifetime. Note, however, that CFC-113 is an extreme case, with growth rates falling from ~15% $year^{-1}$ to zero in the 5 years prior to 1994. For the other species considered here, the corrections and thus errors due to growth are smaller.

Finally, global burdens for all the species (needed in the lifetime calculation) were calculated from global tropospheric and stratospheric observations. The two methods (SF_6-based and CFC-11-based) yield consistent lifetime results for the tracers considered. The determination of absolute (SF_6-based) stratospheric lifetimes in this analysis is limited by the small number of available SF_6 observations in the relevant altitude region. Although more data would certainly help to better constrain the gradient with respect to age, the large curvature in the correlations with age (Figure 6) and the required knowledge of the mass above the tropopause will likely limit the accuracy of absolute lifetime determinations to about 15-20%.

We believe that relative stratospheric lifetimes can in principle be determined to within 5-10%, given a sufficient amount of precise simultaneous observations in the very low stratosphere at midlatitudes. The apparent universality of the correlations in this region suggests that a data set as extensive as the one employed here may not be required. In fact, the observations most relevant for this analysis stem from the ascents and descents of the ER-2 and constitute only a small fraction of the ASHOE/MAESA data set. The measurements needed to determine relative lifetimes accurately might thus well be generated by only a small number of flights sampling the relevant region, that is, altitudes between the tropopause and perhaps 18 km at midlatitudes. Observations from space typically lack the necessary resolution and accuracy in this altitude range. However, the amount of relevant observations has considerably increased during the 1995-1997 Stratospheric Tracers of Atmospheric Transport (STRAT) campaign which, besides ER-2 flights, has included balloon flights providing vertical profiles of SF_6 and several other tracers with a vertical resolution less than 250 m. In addition, a number of long-lived compounds other than the ones considered here have been measured from the ER-2 by whole-air sampling during STRAT. The methods described here may prove useful in improving lifetime estimates for some of those species as well.

Our best estimates for the stratospheric lifetimes of species other than CFC-11 are given in Table 5. They are based on the

Table 5. Best Estimates for Stratospheric Steady State Lifetimes

	Lifetime, years
N_2O	122 ± 24
CH_4	23 ± 18
CFC-12	87 ± 17
CFC-113	100 ± 32
CCl_4	32 ± 6
CH_3CCl_3	34 ± 7
H-1211	24 ± 6

Steady state lifetimes are based on CFC-11 lifetime of 45 ± 7 years (uncertainty of CFC-11 lifetime is included).

correlations with CFC-11 and an assumed CFC-11 lifetime of 45 ± 7 years, a value that we feel better represents the average and uncertainty of current results (including the present SF_6-based estimate of 41 ± 12 years) than the WMO value of 50 ± 5 years. Apart from N_2O and CFC-113 (for which our estimate has a large uncertainty), our best lifetime estimates are significantly (15-33%) shorter than the lifetimes recommended by *WMO* [1995] or used by *IPCC* [1995].

Considering that currently recommended lifetimes for the species regarded here are based almost entirely on 2-D model calculations, our semiempirical estimates provide an independent reference that can be used to test the accuracy of model predictions. Our results may indicate that some of the 2-D models used for the WMO evaluation systematically overestimate lifetimes. The uncertainties of model calculations are often assessed based on agreement between different 2-D models, which is of the order of 20% for the lifetimes considered here. However, the true uncertainties are likely to be greater, since there may be certain shortcomings common to most 2-D models causing similar biases in the results. For example, *Tuck et al.* [1997a] suggest that many models may severely underestimate the strength of the meridional circulation, while *Volk et al.* [1996] point out that 2-D models tend to overestimate the magnitude of horizontal mixing between the tropics and extratropics. Both these biases would lead to model-calculated lifetimes that are too long. In the AER 2-D model [*Ko et al.*, 1985], mixing within the tropics was restricted by decreasing the horizontal eddy diffusion coefficient within the tropical lower stratosphere to yield an entrainment timescale into the tropics of 13.5 months, the value derived by *Volk et al.* [1996] from in situ tracer observations. This adjustment resulted in a ~15% decrease of the calculated lifetimes of tropospheric source gases (R.-L. Shia, submitted to *Journal of Geophysical Research*, 1997), yielding lifetimes closer to the ones derived here. If such a response is symptomatic for 2-D models, then discrepancies between current model-calculated and semiempirically derived lifetimes of the order of 20% should not be too surprising.

If the lifetimes for the chlorinated source gases considered here are indeed as short as found in this work, it would imply a faster recovery of the ozone layer following the phaseout of these substances than currently predicted. Considering that CFC-11, CFC-12, and CCl_4 constitute more than 80% of the anthropogenic chlorine source in the atmosphere, the critical preozone hole atmospheric chlorine content of 2 ppb could be reached some 10 years earlier than the year ~2050 calculated by 2-D models [*WMO*, 1995].

Appendix: Effect of Tracer Transience

Stratospheric mixing ratios of any long-lived tracer may be expressed in terms of the age spectrum by generalizing (6) to allow for chemical loss:

$$\chi(\mathbf{x},t)=\int_0^\infty \chi_0(t-t')G(\mathbf{x},t')L(\mathbf{x},t')dt' \tag{A1}$$

where $L(\mathbf{x},t')$ is an average loss factor for all irreducible elements that took transit paths with transit time t' from the point of stratospheric entry to $\mathbf{x}$. We assume an annual average point of view such that L, just as the age spectrum G, is independent of time. Assessing the average loss factor $L(\mathbf{x},t')$ in detail essentially requires complete knowledge of both stratospheric transport and chemistry. However, we can assert that L must be a monotonically decreasing function in t' with $L = 1$ at $t' = 0$ (no integrated loss at point of stratospheric entry). Note that because there is a unique relation between χ and the mean age Γ (at least in the vicinity of the tropopause that is the region of interest here), all variables in (A1) depend on $\mathbf{x}$ only through $\Gamma(\mathbf{x})$. We therefore may use Γ as independent coordinate instead of $\mathbf{x}$. We further define a loss function $\beta(\Gamma,t')$ such that

$$L(\Gamma,t')=1-\beta(\Gamma,t')t' \tag{A2}$$

where β has units of loss rate (second^{-1}). Substituting this expression into (A1) and evaluating for a steady state tracer with $\chi_0(t) = \sigma_0$ now yields

$$\sigma(\Gamma)=\sigma_0\cdot\left[1-\int_0^\infty G(\Gamma,t')\beta(\Gamma,t')t'dt'\right]. \tag{A3}$$

The loss integral in (A3) describes the decline of mixing ratio with age. In the vicinity of the tropopause ($\Gamma = 0$), $\sigma(\Gamma)$ may be replaced by a first-order Taylor expansion,

$$\sigma(\Gamma)=\sigma_0\cdot(1-\beta_0\Gamma) \tag{A4}$$

where

$$\beta_0\equiv-\frac{1}{\sigma_0}\frac{d\sigma}{d\Gamma}\bigg|_{\Gamma=0}=\frac{d}{d\Gamma}\int_0^\infty G(\Gamma,t')\beta(\Gamma,t')t'dt'\bigg|_{\Gamma=0} \tag{A5}$$

is the normalized gradient of σ with respect to age at the tropopause. Note that replacing $\beta(\Gamma,t')$ with β_0 in (A3) also renders, by means of (7), (A4), suggesting an interpretation for β_0 as an average loss rate for the transit paths contributing to air in the vicinity of the tropopause. In other words, if loss were linear with rate β_0 along all transit paths ending at the tropopause, the same gradient $d\sigma/d\Gamma$ would result as for the complicated loss described by $\beta(\Gamma,t')$. At the tropopause, $\beta(0,t')$ may thus be replaced with the effective linear loss rate β_0.

Next, consider a conserved tracer whose tropospheric time series $\chi_0(t')$ is, for the sake of analogy with (A2), expressed in terms of a growth function $\gamma(t')$ referenced to the time of interest, t:

$$\chi_0(t')=\chi_0(t)\cdot\left(1+\gamma(t-t')\cdot(t'-t)\right). \tag{A6}$$

The stratospheric mixing ratios of this tracer are given by (6), which under substitution of (A6) becomes

$$\chi(\Gamma,t)=\chi_0(t)\cdot\left[1-\int_0^\infty G(\Gamma,t')\gamma(t')t'\,dt'\right] \qquad \text{(A7)}$$

which is the analogous expression to (A3) for a tracer whose decline with age is due to tropospheric growth rather than chemistry. Again, we can expand this expression at the tropopause, defining an average growth rate as

$$\gamma_0 \equiv \frac{d}{d\Gamma}\int_0^\infty G(\Gamma,t')\gamma(t')t'\,dt'\bigg|_{\Gamma=0} . \qquad \text{(A8)}$$

In exact analogy to β_0, γ_0 is the linear growth rate that would create the same gradient $d\chi/d\Gamma$ at the tropopause as the nonlinear growth described by $\gamma(t')$ in (A7).

Finally, consider a tracer experiencing stratospheric loss given by (A2) as well as tropospheric growth given by (A6). Evaluation of its stratospheric mixing ratios by means of (A1) now yields in the vicinity of the tropopause

$$\chi(\Gamma,t)=\chi_0(t)\cdot\left[1-\beta_0\Gamma-\gamma_0\Gamma+\int_0^\infty G(\Gamma,t')\beta(\Gamma,t')\gamma(t')t'^2\,dt\right] \qquad \text{(A9)}$$

This expression describes the decline of mixing ratio with age above the tropopause due to chemistry, growth, and the interaction of chemistry and growth given by the integral term. The mixed term cannot be evaluated exactly without complete knowledge of stratospheric transport and the loss function. However, we can approximate it, by replacing the loss function β and the growth function γ with their effective averages, β_0 and γ_0. This yields, by means of (19),

$$\chi(\Gamma,t)=\chi_0(t)\left[1-\beta_0\Gamma-\gamma_0\Gamma+\beta_0\gamma_0\left(\Gamma^2+2\Delta^2\right)\right] \qquad \text{(A10)}$$

Evaluation of the simple scaling approach described in the text (equation (24)) at the tropopause, using the same terminology, yields the same result, except for the omission of $2\Delta^2$ in the last term; that is, it neglects the interaction of chemistry and growth due to the finite width of the age spectrum. The mixed chemistry-growth term accounts for the fact that for a nonconserved tracer, tropospheric growth will cause a smaller gradient with respect to age than for a conserved one because the older air that entered the stratosphere with lower mixing ratios is also more depleted due to chemical loss, thus contributing less to the overall mixing ratio.

Parameterizing Δ^2 in terms of Γ by means of (20) and recalling that β_0 represents the steady state gradient with respect to age at the tropopause, a relation between the gradients at the tropopause for a transient and a steady state situation is now readily obtained by differentiation of (A10):

$$\left.\frac{d\chi}{d\Gamma}\right|_{\Gamma=0} = -\chi_0(t)\cdot\left(\beta_0+\gamma_0-2\beta_0\gamma_0\Lambda\right) \qquad \text{(A11)}$$

The observed gradient thus consists of the gradients due to only chemistry and only growth minus a correction term due to the interaction of chemistry and growth. Assuming Λ = 1.25 years (compare section 4.1), this mixed chemistry-growth term is negligible only compared to γ_0 if $\beta_0\cdot$(2.5 years) << 1, that is, if insignificant loss occurred in air with ages of 2.5 years. Figure 6 reveals that this is the case only for the longest lived species considered. The simple scaling approach of (24), which neglects the mixed term, is therefore not generally applicable for the tracers considered here. Substituting $\beta_0 = -(d\sigma/d\Gamma)/\sigma_0$ and $\chi_0(t) = \sigma_0$ in (A11) and solving for $d\sigma/d\Gamma$ yields (25) in the text.

The only missing piece in the growth correction is now the effective linear growth rate γ_0. Its derivation is straightforward for a quadratic tropospheric time series, expanded around the time of interest t:

$$\chi_0(t')=\chi_0(t)\cdot\left[1+b\cdot(t'-t)+c\cdot(t'-t)^2\right] \qquad \text{(A12)}$$

in which case the growth function (as defined in equation (A6)) is $\gamma(t') = b - ct'$, and evaluation of (A8) yields the result quoted in the text

$$\gamma_0=\frac{d}{dt}\left[b\Gamma-c\cdot\left(\Gamma^2+2\Delta^2\right)\right]_{\Gamma=0}=b-2\Lambda c \qquad \text{(A13)}$$

where the spectral width Δ was again parameterized in terms of Γ using (20).

Acknowledgments. We are indebted to S.A. Montzka, J.H. Butler, T.M. Thompson, and E.J. Dlugokencky for providing tropospheric data, to R.J. Salawitch for facilitating the use of ATMOS data, to C. Appenzeller for the calculation of the stratospheric mass, to P.J. Fraser, L.P. Steele, and M.P. Lucarelli for support during the field deployments in New Zealand, and to P.R. Wamsley for helping with the processing of ACATS data. C.M.V. has greatly benefited from correspondence and discussions with T.M. Hall, D.W. Waugh, and F.L. Moore. Comments on the original manuscript by S.W. Wofsy, R.A. Plumb, and I. Plumb are much appreciated. We finally extend thanks to our many colleagues who made the 1994 ASHOE/MAESA campaign a success, especially the pilots of the ER-2 aircraft. This research is supported in part by NASA's Upper Atmospheric Research Program (UARP), the Atmospheric Effects of Stratospheric Aircraft (AESA) component of the NASA High-Speed Research Program (HSRP), and the Atmospheric Chemistry Project of NOAA's Climate and Global Change Program.

References

Appenzeller, C., J.R. Holton, and K.H. Rosenlof, Seasonal variation of mass transport across the tropopause, *J. Geophys. Res.*, *101*, 15,071-15,078, 1996.

Avallone, L.M., and M.J. Prather, Photochemical evolution of ozone in the lower tropical stratosphere, *J. Geophys. Res.*, *101*, 1457-1461, 1996.

Bischof, W., R. Borchers, P. Fabian, and B.C. Krüger, Increased concentration and vertical distribution of carbon dioxide in the stratosphere, *Nature*, *316*, 708-710, 1985.

Boering, K.A., B.C. Daube Jr., S.C. Wofsy, M. Loewenstein, J.R. Podolske, and E.R. Keim, Tracer-tracer relationships and lower stratospheric dynamics: CO_2 and N_2O correlations during SPADE, *Geophys. Res. Lett.*, *21*, 2567-2570, 1994.

Boering, K.A., S.C. Wofsy, B.C. Daube, H.R. Schneider, M. Loewenstein, J.R. Podolske, and T.J. Conway, Stratospheric mean ages and transport rates from observations of carbon dioxide and nitrous oxide, *Science*, *274*, 1340-1343, 1996.

Butler, J.H., J.W. Elkins, B.D. Hall, S.O. Cummings, and S.A. Montzka, A decrease in the growth rates of atmospheric halon concentrations, *Nature*, *359*, 403-405, 1992.

Butler, J.H., S.A. Montzka, A.D. Clarke, J.M. Lobert, and J.W. Elkins, Growth and distribution of halons in the atmosphere, *J. Geophys. Res.*, in press, 1997.

Chang, A.Y., et al., A comparison of measurements from ATMOS and instruments aboard the ER-2 aircraft: Tracers of atmospheric transport, *Geophys. Res. Lett.*, *23*, 2389-2392, 1996.

Crewell, S., C. Dongjie, R.L. de Zafra, and C. Trimble, Millimeter wave spectroscopic measurements over the South Pole, 1, A study of stratospheric dynamics using N_2O observations, *J. Geophys. Res.*, *100*, 20,839-20,844, 1995.

Crutzen, P.J., The influence of nitrogen oxides on the atmospheric ozone content, *Q. J. R. Meteorol. Soc.*, *96*, 320-325, 1970.

Cunnold, D.M., P.J. Fraser, R.F. Weiss, R.G. Prinn, P.G. Simmonds, B.R. Miller, F.N. Alyea, and A.J. Crawford, Global trends and annual releases of CCl_3F and CCl_2F_2 estimated from ALE/GAGE and other measurements from July 1978 to June 1991, *J. Geophys. Res.*, *99*, 1107-1126, 1994.

Cunnold, D.M., R.F. Weiss, R.G. Prinn, D. Hartley, P.G. Simmonds, P.J. Fraser, B. Miller, F.N. Alyea, and L. Porter, GAGE/AGAGE measurements indicating reductions in global emissions of CCl_3F and CCl_2F_2 in 1992-1994, *J. Geophys. Res.*, *102*, 1259-1269, 1997.

Daniel, J.S., S.M. Schauffler, W.H. Pollock, S. Solomon, A. Weaver, L.E. Heidt, R.R. Garcia, E.L. Atlas, and J.F. Vedder, On the age of stratospheric air and inorganic chlorine and bromine release, *J. Geophys. Res.*, *101*, 16,757-16,770, 1996.

Dlugokencky, E.J., L.P. Steele, P.M. Lang, and K.A. Masarie, The growth rate and distribution of atmospheric methane, *J. Geophys. Res.*, *99*, 17,021-17,043, 1994.

Efron, B., and R. Tibshirani, Statistical data analysis in the computer age, *Science*, *253*, 390-395, 1991.

Ehhalt, H.D., P.E. Röth, and U. Schmidt, On the temporal variance of stratospheric trace gas concentrations, *J. Atmos. Chem.*, *1*, 27-51, 1983.

Elkins, J.W., T.M. Thompson, T.H. Swanson, J.H. Butler, B.D. Hall, S.O. Cummings, D.A. Fisher, and A.G. Raffo, Decrease in the growth rates of atmospheric chlorofluorocarbons 11 and 12, *Nature*, *364*, 780-783, 1993.

Elkins, J.W., et al., Airborne gas chromatograph for in situ measurements of long-lived species in the upper troposphere and lower stratosphere, *Geophys. Res. Lett.*, *23*, 347-350, 1996a.

Elkins, J.W., et al., Nitrous Oxide and Halocompounds, in *Climate Monitoring and Diagnostics Laboratory No. 23 - Summary Report 1994-1995*, edited by D.J. Hofmann, T.J. Peterson, and R.M. Rosson, pp. 84-111, U.S. Dep. of Commer., Boulder, Colo., 1996b.

Fahey, D.W., S. Solomon, S.R. Kawa, M. Loewenstein, J.R. Podolske, S.E. Strahan, and K.R. Chan, A diagnostic for denitrification in the winter polar stratospheres, *Nature*, *345*, 698-702, 1990.

Fahey, D.W., et al., In situ observations of NO_y, O_3, and the NO_y/O_3 ratio in the lower stratosphere, *Geophys. Res. Lett.*, *23*, 1653-1656, 1996.

Fisher, D.A., and P.M. Midgley, Uncertainties in the calculation of atmospheric releases of chlorofluorocarbons, *J. Geophys. Res.*, *99*, 16,643-16,650, 1994.

Fisher, D.A., C.H. Hales, W.-C. Wang, M.K.W. Ko, and N.D. Sze, Model calculations of the relative effects of CFCs and their replacements on global warming, *Nature*, *433*, 513-516, 1990.

Fraser, P., D. Cunnold, F. Alyea, R. Weiss, R. Prinn, P. Simmonds, B. Miller, and R. Langenfelds, Lifetime and emission estimates of 1,1,2-trichlorotrifluorethane (CFC-113) from daily global background observations June 1982 to June 1994, *J. Geophys. Res.*, *101*, 12,585-12,599, 1996.

Geller, L.S., J.W. Elkins, J.M. Lobert, A.D. Clarke, D.H. Hurst, J.H. Butler, and R.C. Myers, Tropospheric SF_6: Observed latitudinal distribution and trends, derived emissions and interhemispheric exchange time, *Geophys. Res. Lett.*, *24*, 675-678, 1997.

Gunson, M.R., et al., The Atmospheric Trace Molecule Spectroscopy (ATMOS) experiment: Deployment on the ATLAS space shuttle missions, *Geophys. Res. Lett.*, *23*, 2333-2336, 1996.

Hall, T.M., and R.A. Plumb, Age as a diagnostic of stratospheric transport, *J. Geophys. Res.*, *99*, 1059-1070, 1994.

Hall, T.M., and M.J. Prather, Simulations of the trend and annual cycle in stratospheric CO_2, *J. Geophys. Res.*, *98*, 10,573-10,581, 1993.

Hall, T.M., and M.J. Prather, Seasonal evolutions of N_2O, O_3, and CO_2: Three-dimensional simulations of stratospheric correlations, *J. Geophys. Res.*, *100*, 16,699-16,720, 1995.

Hall, T.M., and D. Waugh, Tracer transport in the tropical stratosphere due to vertical diffusion and horizontal mixing, *Geophys. Res. Lett.*, *24*, 1383-1386, 1997.

Harnisch, J., R. Borchers, P. Fabian, and M. Maiss, Tropospheric trends for CF_4 and C_2F_6 since 1982 derived from SF_6 dated stratospheric air, *Geophys. Res. Lett.*, *23*, 1099-1102, 1996.

Hoerling, M.P., T.K. Schaack, and A.J. Lenzen, Global objective tropopause analysis, *Mon. Weather Rev.*, *119*, 1816-1831, 1991.

Holton, J. R., A dynamically based transport parameterization for one-dimensional photochemical models of the stratosphere, *J. Geophys. Res.*, *91*, 2681-2686, 1986.

Intergovernmental Panel on Climate Change (IPCC), *Climate Change 1994: Radiative Forcing of Climate Change and An Evaluation of the IPCC 1992 Emission Scenarios*, edited by J. T. Houghton, et al., 339 pp., Cambridge Univ. Press, New York, 1995.

Johnston, H.S., O. Serang, and J. Podolske, Instantaneous global nitrous oxide photochemical rates, *J. Gepohys. Res.*, *84*, 5077-5082, 1979.

Kaye, J.A., S.A. Penkett, and F.M. Ormond (Eds.), Report on concentrations, lifetimes, and trends of CFCs, halons, and related species, *NASA Ref. Publ.*, *1339*, 1994.

Ko, M.K.W., and N.D. Sze, A 2-D model calculation of atmospheric lifetimes for N_2O, CFC-11 and CFC-12, *Nature*, *297*, 317-319, 1982.

Ko, M.K.W., K.K. Tung, D.K. Weisenstein, and N.D. Sze, A zonal mean model of stratospheric tracer transport in isentropic coordinates: Numerical simulations for nitrous oxide and nitric acid, *J. Geophys. Res.*, *90*, 2313-2329, 1985.

Ko, M.K.W., N.D. Sze, and D.K. Weisenstein, Use of satellite data to constrain the model-calculated atmospheric lifetime for N_2O: Implications for other trace gases, *J. Geophys. Res.*, *96*, 7547-7552, 1991.

Lee, J.M., W.T. Sturges, S.A. Penkett, D.E. Oram, U. Schmidt, A. Engel, and R. Bauer, Observed stratospheric profiles and stratospheric lifetimes of HCFC-141b and HCFC-142b, *Geophys. Res. Lett.*, *22*, 1369-1372, 1995.

Mahlman, J.D., I.I. H. Levy, and W.J. Moxim, Three-dimensional simulations of stratospheric N_2O: Predictions for other trace constituents, *J. Geophys. Res.*, *91*, 2687-2707, 1986.

Maiss, M., L.P. Steele, R.J. Francey, P.J. Fraser, R.L. Langenfelds, N.B.A. Trivett, and I. Levin, Sulfur hexafluoride - A powerful new atmospheric tracer, *Atmos. Environ.*, *30*, 1621-1629, 1996.

McIntyre, M.E., and T.N. Palmer, Breaking planetary waves in the stratosphere, *Nature*, *305*, 593-600, 1983.

Michelsen, H.A., G.L. Manney, M.R. Gunson, M.C. Abrams, C.P. Rinsland, A.Y. Chang, and S.C. Wofsy, Latitude-dependent tracer relationships from ATMOS/ATLAS-3, paper presented at the Annual Meeting: The Atmospheric Effects of Aviation, NASA Office of Aeronautics, Virginia Beach, Va., June 1995.

Minschwaner, K., R.J. Salawitch, and M.B. McElroy, Absorption of solar radiation by O_2: Implications for O_3 and lifetimes of N_2O, $CFCl_3$, and CF_2Cl_2, *J. Geophys. Res.*, *98*, 10,543-10,561, 1993.

Minschwaner, K., A.E. Dessler, J.W. Elkins, C.M. Volk, D.W. Fahey, M. Loewenstein, J.R. Podolske, A.E. Roche, and K.R. Chan, Bulk properties of isentropic mixing into the tropics in the lower stratosphere, *J. Geophys. Res.*, *101*, 9433-9439, 1996.

Molina, M.J., and F.S. Rowland, Stratospheric sink for chlorofluoromethanes: Chlorine atom catalyzed destruction of ozone, *Nature*, *249*, 810-814, 1974.

Montzka, S.A., J.H. Butler, R. C. Myers, T.M. Thompson, T.H. Swanson, A.D. Clarke, L.T. Lock, and J.W. Elkins, Decline in the tropospheric abundance of halogen from halocarbons: Implications for stratospheric ozone depletion, *Science*, *272*, 1318-1322, 1996.

Murgatroyd, R.J., and A. O'Neill, Interaction between the troposphere and stratosphere, *Philos. Trans. R. Soc. London, Ser. A*, *296*, 87-102, 1980.

Murphy, D.M., S.W. Fahey, M.H. Proffitt, S.C. Liu, K.R. Chan, C.S. Eubank, S.R. Kawa, and K.K. Kelly, Reactive nitrogen and its correlation with ozone in the lower stratosphere and upper troposphere, *J. Geophys. Res.*, *98*, 8751-8773, 1993.

Patra, K.P., L. Lal, B.H. Subbaraya, C.H. Jackman, and P. Rajaratnam, Observed vertical profile of sulphur hexafluoride (SF_6) and its atmospheric applications, *J. Geophys. Res.*, *102*, 8855-8859, 1997.

Plumb, R.A., A "tropical pipe" model of stratospheric transport, *J. Geophys. Res.*, *101*, 3957-3972, 1996.

Plumb, R.A., and M.K.W. Ko, Interrelationships between mixing ratios of long-lived stratospheric constituents, *J. Geophys. Res.*, *97*, 10,145-10,156, 1992.

Plumb, R.A., and D.D. McConalogue, On the meridional structure of long-lived tropospheric constituents, *J. Geophys. Res.*, *93*, 15,897-15,913, 1988.

Podolske, J., and M. Loewenstein, Airborne tunable diode laser spectrometer for trace-gas measurement in the lower stratosphere, *Appl. Opti.*, *32*, 5324-5333, 1993.

Pollock, W.H., L.E. Heidt, R.A. Lueb, J.F. Vedder, M.J. Mills, and S. Solomon, On the age of stratospheric air and ozone depletion potentials in polar regions, *J. Geophys. Res.*, *97*, 12,993-12,999, 1992.

Prather, M.J., M.B. McElroy, S.C. Wofsy, G. Russell, and D. Rind, Chemistry of the global troposhere: Fluorocarbons as tracers of air motion, *J. Geophys. Res.*, *92*, 6579-6613, 1987.

Press, W.H., S.A. Teukolsky, W.T. Vetterling, and B.P. Flannery, *Numerical Recipes in C: The Art of Scientific Computing*, Cambridge Univ. Press, New York, 1992.

Prinn, R.G., R.F. Weiss, B.R. Miller, J. Huang, F.N. Alyea, D.M. Cunnold, P.J. Fraser, D.E. Hartley, and P.G. Simmonds, Atmospheric trends and lifetime of CH_3CCl_3 and global OH concentrations, *Science*, *269*, 187-192, 1995.

Proffitt, M.H., D.W. Fahey, K.K. Kelly, and A.F. Tuck, High-latitude ozone loss outside the Antarctic ozone hole, *Nature*, *342*, 233-237, 1989.

Proffitt, M.H., J.J. Margitan, K.K. Kelly, M. Loewenstein, J.R. Podolske, and K.R. Chan, Ozone loss in the Arctic polar vortex inferred from high-altitude aircraft measurements, *Nature*, *347*, 31-36, 1990.

Randel, W.J., J.C. Gille, A.E. Roche, J.B. Kumer, J.L. Mergenthaler, J.W. Waters, E.F. Fishbein, and W.A. Lahoz, Stratospheric transport from the tropics to middle latitudes by planetary-wave mixing, *Nature*, *365*, 533-535, 1993.

Ravishankara, A.R., S. Solomon, A.A. Turnipseed, and R.F. Warren, Atmospheric lifetimes of long-lived halogenated species, *Science*, *259*, 194-199, 1993.

Reiter, E.R., Stratospheric-tropospheric exchange processes, *Rev. Geophys.*, *13*, 459-474, 1975.

Rosenlof, K.H., and J.R. Holton, Estimates of the stratospheric residual circulation using the downward control principle, *J. Geophys. Res.*, *98*, 10,465-10,479, 1993.

Schmidt, U., and A. Khedim, In situ measurements of carbon dioxide in the winter Arctic vortex and at midlatitudes: An indicator of the "age" of stratospheric air, *Geophys. Res. Lett.*, *18*, 763-766, 1991.

Schmidt, U., R. Bauer, A. Khedim, E. Klein, G. Kulessa, and B. Schubert, In situ observations of long-lived trace gases in the Arctic stratosphere during winter, in *Ozone in the Atmosphere*, edited by R.D. Bojkov and P. Fabian, pp. 298-301, A. Deepak, Hampton, Va., 1989.

Solomon, S., M. Mills, L.E. Heidt, W.H. Pollock, and A.F. Tuck, On the evaluation of ozone depletion potentials, *J. Geophys. Res.*, *97*, 825-842, 1992.

Tans, P.P., et al., Carbon Cycle, in *Climate Monitoring and Diagnostics Laboratory No. 23 - Summary Report 1994-1995*, edited by D.J. Hofmann, T.J. Peterson, and R.M. Rosson, pp. 29-49, NOAA, Boulder, Colo., 1996.

Trenberth, K.E., and C.J. Guillemot, The total mass of the atmosphere, *J. Geophys. Res.*, *99*, 23,079-23,088, 1994.

Trepte, C.R., and M.H. Hitchman, Tropical stratospheric circulation deduced from satellite aerosol data, *Nature*, *355*, 626-628, 1992.

Tuck, A.F., et al., The Brewer Dobson circulation in the light of high altitude in situ aircraft observations, *Q. J. R. Meteorol. Soc.*, *123*, 1, 1997a.

Tuck, A.F., W.H. Brune, and R.S. Hipskind, Airborne Southern Hemisphere Ozone Experiment/Measurements for Assessing the Effects of Stratospheric Aircraft (ASHOE/MAESA): A road map, *J. Geophys. Res.*, *102*, 3901-3904, 1997b.

Volk, C.M., Stratospheric transport and tracer lifetimes from airborne in situ observations, Ph.D. thesis, Univ. of Colo., Boulder, 1996.

Volk, C.M., et al., Quantifying transport between the tropical and midlatitude lower stratosphere, *Science*, *272*, 1763-1768, 1996.

Warneck, P., *Chemistry of the Natural Atmosphere*, 757 pp., Academic, San Diego, Calif., 1988.

Waugh, D.W., et al., Mixing of polar vortex air into middle latitudes as revealed by tracer-tracer scatter plots, *J. Geophys. Res.*, *102*, 13,119-13,134, 1997a.

Waugh, D.W., et al., Three-dimensional simulations of long-lived tracers using winds from MACCM2, *J. Geophys. Res.*, in press, 1997b.

World Meteorological Organization (WMO), *Scientific assessment of ozone depletion: 1991*, *Rep. 25*, Global Ozone Res. and Monit. Proj., Geneva, 1992.

World Meteorological Organization (WMO), *Scientific assessment of ozone depletion: 1994*, *Rep. 37*, Global Ozone Res. and Monit. Proj., Geneva, 1995.

Woodbridge, E.L., et al., Estimates of total organic and inorganic chlorine in the lower stratosphere from in situ and flask measurements, *J. Geophys. Res.*, *100*, 3057-3064, 1995.

Wuebbles, D.J., Chlorocarbon emission scenarios: Potential impact on stratospheric ozone, *J. Geophys. Res.*, *88*, 1433-1443, 1983.

K. R. Chan, M. Loewenstein, and J. R. Podolske, NASA Ames Research Center, Moffett Field, CA 94035. (e-mail: podolske@ames.arc.nasa.gov)

G. S. Dutton and J. W. Elkins, Climate Monitoring and Diagnostics Laboratory, National Oceanic and Atmospheric Administration (NOAA), 325 Broadway, Boulder, CO 80303. (e-mail: gdutton@cmdl.noaa.gov; jelkins@cmdl.noaa.gov)

D. W. Fahey, NOAA Aeronomy Laboratory, 325 Broadway, Boulder, CO 80303. (e-mail: dfahey@al.noaa.gov)

J. M. Gilligan, Department of Physics and Astronomy, Vanderbilt University, Nashville, TN 37203. (e-mail: jonathon.gilligan@vanderbilt.edu)

M. R. Gunson, Jet Propulsion Laboratory, California Institute of Technology, Pasadena, CA 91109. (email: mrg@atmosmips.jpl.nasa.gov)

C. M. Volk (corresponding author), Instut fur Meteorologie und Geophysik, Universitat Franfurt, Georg-Voigt-Str. 14, 60323 Frankfurt am Main, Germany. (e-mail: M.Volk@meteor.uni-frankfurt.de)

(Received February 11, 1997; revised July 24, 1997; accepted July 31, 1997.)